PHYSICAL REVIEW D **95,** 043524 (2017)

Production of heavy sterile neutrinos from vector boson decay at electroweak temperatures

Louis Lello,[1,2,*] Daniel Boyanovsky,[1,†] and Robert D. Pisarski[2,3,‡]

[1]*Department of Physics and Astronomy, University of Pittsburgh, Pittsburgh, Pennsylvania 15260, USA*
[2]*Department of Physics, Brookhaven National Laboratory, Upton, New York 11973, USA*
[3]*RIKEN/BNL Research Center, Brookhaven National Laboratory, Upton, New York 11973, USA*

(Received 24 September 2016; published 22 February 2017)

In the standard model extended with a seesaw mass matrix, we study the production of sterile neutrinos from the decay of vector bosons at temperatures near the masses of the electroweak bosons. We derive a general quantum kinetic equation for the production of sterile neutrinos and their effective mixing angles, which is applicable over a wide range of temperature, to all orders in interactions of the standard model and to leading order in a small mixing angle for the neutrinos. We emphasize the relation between the production rate and Landau damping at one-loop order and show that production rates and effective mixing angles depend sensitively upon the neutrino's helicity. Sterile neutrinos with positive helicity interact more weakly with the medium than those with negative helicity, and their effective mixing angle is not modified significantly. Negative helicity states couple more strongly to the vector bosons, but their mixing angle is strongly suppressed by the medium. Consequently, if the mass of the sterile neutrino is $\lesssim$8.35 MeV, there are fewer states with negative helicity produced than those with positive helicity. There is an Mikheyev-Smirnov-Wolfenstein-type resonance in the absence of lepton asymmetry, but due to screening by the damping rate, the production rate is not enhanced. Sterile neutrinos with negative helicity freeze out at $T_f^- \simeq 5$ GeV, whereas positive helicity neutrinos freeze out at $T_f^+ \simeq 8$ GeV, with both distributions far from thermal. As the temperature decreases, due to competition between a decreasing production rate and an increasing mixing angle, the distribution function for states with negative helicity is broader in momentum and hotter than that for those with positive helicity. Sterile neutrinos produced via vector boson decay do not satisfy the abundance, lifetime, and cosmological constraints to be the sole dark matter component in the Universe. Massive sterile neutrinos produced via vector boson decay might solve the ^{7}Li problem, albeit at the very edge of the possible parameter space. A heavy sterile neutrino with a mass of a few MeV could decay into light sterile neutrinos, of a few keV in mass, that contribute to warm dark matter. We argue that heavy sterile neutrinos with lifetime $\leq 1/H_0$ reach local thermodynamic equilibrium.

DOI: 10.1103/PhysRevD.95.043524

I. INTRODUCTION

The paradigm of standard cosmology is inflation plus cold dark matter, ΛCDM. While it succeeds in describing the formation of structure at large scales, there are discrepancies at smaller scales, especially galactic and subgalactic. There is the core-cusp problem: N-body simulations of cold dark matter produce dark matter profiles that generically feature cusps, yet observations suggest that the profile has a smooth core [1,2]. There is also the missing satellites problem, where simulations also predict that typical galaxies are surrounded by satellites dominated by dark matter, which is inconsistent with current observations [3]. Both of these problems can be solved by allowing some fraction of the dark matter to be warm dark matter (WDM) [4–9]. A possible candidate for warm dark matter is a massive "sterile" neutrino [10–17]. Whether dark matter is hot or cold depends upon its free streaming length, λ_{fs}, which is the cutoff scale in the linear power spectrum of density perturbations. Cold dark matter with $\lambda_{fs} \lesssim$ pc produces cuspy profiles, while warm dark matter with $\lambda_{fs} \sim$ few kpc gives cored profiles.

One important question is whether these discrepancies can be explained with the standard ΛCDM model by including the effects of baryons in the simulations. Recent simulations of warm dark matter which include velocity dispersion suggest that cores do form, but do not yet reliably constrain, the mass of the WDM candidate in a model independent manner [18].

In order to evade cosmological bounds, the distribution functions of warm dark matter cannot be thermal [19]. How sterile neutrinos are produced in the early Universe was studied originally in Refs. [20,21]. In Refs. [11,22–27], it was argued that sterile neutrinos are a viable candidate for warm dark matter, which is produced out of local equilibrium either nonresonantly [11,20,23,25] or resonantly in the presence of a lepton asymmetry [22]. Models in which a

*lal81@pitt.edu
†boyan@pitt.edu
‡pisarski@bnl.gov

scalar decays into a pair of sterile neutrinos at the electroweak scale (or higher) also yields a nonthermal distribution [28–32]. Observations of the x-ray emission spectrum of the Andromeda galaxy with Chandra led to tight constraints on the nonresonant production of sterile neutrinos [33]. More recently, the report of observation of a 3.5 keV signal from the XMM Newton x-ray telescope has been argued to be due to a 7 keV sterile neutrino [34,35], although this interpretation has been challenged [36–39]. The prospect of a keV sterile dark matter candidate continues to motivate studies in both theory and observation [27,29,31,40–47].

Neutrino masses, mixing and oscillations are uncontroversial evidence of physics beyond the standard model. A robust experimental program has brought measurements of most of the parameters associated with light neutrino masses [48,49] with several relevant questions poised to be answered in the near future [50]. Short baseline neutrino oscillation experiments such as LSND and MiniBooNE [51,52] present a picture of the neutrino sector which may require an additional sterile neutrino species of mass $\sim$1 eV [15,53,54], but there remains tension with other experiments [55], and a definitive resolution of these anomalies requires further experiments [56–61]. An interpretation of short baseline experimental anomalies as a signal for sterile neutrinos leads to a relatively light mass $\sim$eV which rules out this putative new sterile neutrino as a candidate for dark matter. However, many well-motivated extensions beyond the standard model posit the existence of heavy neutrinos. It has been argued that sterile neutrinos with a mass on the order of MeV or larger [62] could decay and explain the short baseline anomalies. Alternatively, heavy sterile neutrinos produced through rare decay channels could also explain the anomaly [63]. Recent proposals make the case for a program to search for heavy neutrinos [64,65] in a wide range of experiments including hadron colliders [66–71]. Furthermore, it has been argued that heavy sterile neutrinos in the mass range 100–500 MeV can decay nonthermally and so evade bounds from cosmology and accelerator experiments [72]. Sterile neutrinos with mass $\simeq$MeV can be of cosmological relevance in models where the reheating temperature is low [73].

A heavy sterile neutrino with mass $\simeq$14 MeV, a mixing angle $\theta \simeq 10^{-3}$, and a lifetime $\tau_s \simeq 1.8 \times 10^5$ s has been proposed [74] as a novel solution to the "lithium problem." This is the nearly threefold discrepancy between the standard big bang nucleosynthesis (BBN) prediction and observed abundance of ^{7}Li [74–78]. This solution relies on the energy injected by the decay of the sterile neutrino to destroy part of ^{7}Be prior to its conversion into ^{7}Li in the late stages of BBN [74,78]. This mechanism has been recently reanalyzed and confirmed in Ref. [79] with a sterile neutrino mass $\simeq$4.35 MeV, mixing angle $\theta \leq 10^{-5}$–10^{-4} and lifetime $\simeq 1.8 \times 10^5$ s. An important bonus of this mechanism is that the decay of the heavy sterile neutrino, $\simeq$MeV in mass, yields an *increase* in the effective number of relativistic species $\Delta N_{\rm eff} \simeq 0.34$ at the 95% C.L. [79]. The energy injection from the decay of heavy sterile neutrinos with longer lifetime may also contribute to early ionization [80]. Although there is no experimental evidence for such heavy sterile neutrinos, there are stringent accelerator and cosmological bounds on their possible masses and mixing angles with active neutrinos [73,81–83].

There is a hierarchy of masses for the light active neutrinos, with nearly 2 orders of magnitude between the mass squared differences for the explanation of solar and atmospheric neutrino mixing.

Possible extensions beyond the standard model may also accommodate a hierarchy of *heavy* neutrinos [17,84,85].

Current and future underground neutrino detectors may be able to probe dark matter candidates with $\simeq$few MeV [86]. The possibility of a hierarchy of heavy sterile neutrinos offers novel production mechanisms for warm (and hot) dark matter, from the cascade decays of heavy neutrinos to lighter ones. This possibility is similar to models of many dark matter components proposed recently [87], where the decay of a heavy field seeds the production of a light one. This leads to a scenario of *mixed dark matter* described by several species of massive neutrinos with nonequilibrium distribution functions and thereby evades Lyman-α constraints [88]. A recent article argued on various possible production mechanisms of sterile neutrino directly from standard model processes available throughout the thermal history of the Universe and analyzed in detail the scenario of production of mixed dark matter (colder, warmer and hotter) from pion decay shortly after the QCD crossover [89].

This analysis, along with previous work [45], also suggests that the decay of a heavy sterile neutrino into a light active neutrino increases the effective number of neutrinos, $N_{\rm eff}$. This has been studied recently in Ref. [79] in the context of energy injection post (BBN) from the decay of a heavy sterile neutrino with lifetime $\simeq 10^5$ secs.

A. Motivation and goals

Sterile neutrinos with masses in the range KeV–few MeV may play an important role in cosmology.

Most of the studies of their production and freeze-out have focused on the well-motivated mass range of few KeV as possible warm dark matter candidates. However, if the hierarchy of masses and mixing of light active neutrinos is of any guide in extensions beyond the standard model, a possible hierarchy of heavier sterile neutrinos that mix with the light active neutrinos, with very small mixing angles, may emerge.

In this scenario, the possibility that heavier neutrinos yield a mixture of dark matter components, from cold, heavy species to warm, light ones, with important cosmological impact, and the possibility that $\simeq$MeV sterile neutrinos *may* yield a solution to the ^{7}Li problem

[74,78,79] motivates our study of the production and freeze-out of sterile neutrinos in a wider range of masses and temperatures. In this article, we study the production of sterile neutrinos solely from *standard model interactions*. Reference [89] identified several possible processes available throughout the thermal history of the Universe that may lead to the production of a sterile species from its mixing with active neutrinos.

Recently, Ref. [26] studied the damping rate of GeV sterile neutrinos at high temperature within the context of the washout rate of leptonic densities.

In contrast, we focus on sterile neutrinos with masses $\lesssim$ few MeV, which is appropriate both to dark matter and the possible solution of the ^{7}Li problem. We highlight the important role which different helicity channels play for the production rate and mixing angles, including cosmological expansion. We also compute the nonequilibrium distribution functions for different helicities, along with various cosmological constraints.

In this article, our goals are twofold:

(i) Using quantum kinetics, we seek to provide a consistent description of both production and freeze-out, valid in a wide range of temperature, under a minimal set of assumptions. These are as follows: (a) Except for the coupling between sterile and active neutrinos via a seesaw-type mass matrix, we only consider the interactions of the standard model. (b) Consistent with bounds from accelerator experiments and cosmology [33–35,43,73,81–83], we assume that the vacuum mixing angle $\theta \ll 1$. Taken together, these bounds suggest that $\theta^2 \lesssim 10^{-5}$ for a wide range of masses $M_s \lesssim 300$ MeV. (c) Interactions in the standard model can be treated perturbatively, and the relevant degrees of freedom, including active neutrinos, are in local thermal equilibrium (LTE) during both production and freeze-out of sterile species. The latter is consistent with a small mixing angle.

(ii) We work to leading order in the electroweak coupling α_W, without any assumption on the mass scales of the sterile neutrinos. To leading order in α_W, the production of sterile neutrinos occurs from the decay of W and Z bosons in the thermal bath.

We focus on the temperatures at the electroweak scale, $T \simeq M_W, M_Z$. This is sufficiently below the temperature for the electroweak phase transition, which is a crossover at $T_{ew} \simeq 160$ GeV [25], so that the W and Z bosons are in local thermal equilibrium, with masses close to those at zero temperature.

B. Brief summary of results

For simplicity, we consider a model with one active and one sterile neutrino. Our main results are as follows:

(i) We obtain the mass eigenstates, effective mixing angles and damping rates directly from the equations of motion in the medium in terms of the full self-energy *to all orders in weak interactions*. We give an expression for the effective mixing angles which is broadly valid for $\theta \ll 1$ and to all orders in perturbation theory in standard model couplings, at any temperature. The mixing angle in the medium depends strongly on helicity; negative helicity neutrinos (and positive helicity antineutrinos) feature mixing angles which are strongly suppressed at high temperature. In contrast, for positive helicity neutrinos (and negative helicity anti-neutrinos), the corrections to the mixing angle are subleading, so the effective mixing angle is nearly the same as that in vacuum. This happens because the interaction of neutrinos with positive helicity is helicity suppressed. Damping rates are also helicity dependent and suppressed for those with positive helicity; however, because the effective mixing angle is *larger* than that of the negative helicity states, the resulting production rate is comparable in a wide range of masses. We obtain the general form of the quantum kinetic equation that describes the production and freeze-out of sterilelike neutrinos The production rate is determined by the damping rate of sterilelike *mass eigenstates* and the mixing angle in the medium. Although the production rate of positive helicity states is suppressed by helicity, it is comparable to the rate for those with negative helicity, because over a wide regime of masses, it is compensated by the suppression of the mixing angle for neutrinos with negative helicity.

(ii) For sterilelike masses $M_s \ll M_W$, we find a Mikheyev-Smirnov-Wolfenstein (MSW) [90] resonance in the *absence of a leptonic asymmetry*. However, it is screened by the damping rate and so does *not* lead to enhanced production. For this mass range of M_s, negative helicity states freeze out at $T_f^- \simeq 5$ GeV, whereas positive helicity states freeze out at $T_f^+ \simeq 8$ GeV. Both feature highly nonthermal distribution functions, where for the negative helicity states the distribution function is broader and hotter than that for positive helicity.

Paradoxically, this is a consequence of a *longer freeze-out time* for the negative helicity states, despite the fact that their coupling to the environment is stronger. This is a surprising result, stemming from a competition between a diminishing damping rate and an *increasing* effective mixing angle as the temperature decreases. We argue that this leading order production mechanism establishes a *lower bound* for the abundance. We find, however, that sterilelike neutrinos produced via vector boson decay do not satisfy the various bounds on lifetimes and mixing angles to be viable keV dark matter candidates. However, they can be suitable as the MeV sterile neutrinos that are conjectured to provide a solution to

the ^{7}Li problem. This is with the caveat that there seems to be tension among the various bounds available in the literature [79,83]. Just as these heavier neutrinos may decay by injecting energy into the plasma as the solution to this problem, we also conjecture that they may also decay into lighter $\simeq$KeV sterile neutrinos, with a much smaller branching ratio, that could be suitable candidates for warm dark matter.

To the best of our knowledge, there has not yet been a systematic study of the full dynamics of production and freeze-out obtaining the nonequilibrium distribution functions of heavy sterile neutrinos with $M_s \lesssim$ few MeV at the scale $T \simeq 100$ GeV with cosmological expansion. Our analysis is motivated by the possible cosmological relevance of sterile neutrinos in a wide range of masses and complements previous studies that focus on lower temperature regimes.

II. MASS EIGENSTATES, DAMPING RATES AND MIXING ANGLES IN THE MEDIUM

We consider the standard model with only one leptonic generation, one active neutrino and its charged lepton partner and one $SU(2)$ singlet Dirac sterile neutrino within a type-I seesaw scenario [91], to discuss the main aspects in the simplest setting. This choice differs from other versions of the type-I seesaw that include only a right-handed Majorana neutrino. The important difference is that in the Majorana case there is no antineutrino contribution, and quantitatively this results in an overall factor $1/2$ in the final abundances.

With one lepton doublet $L_L = (\nu_{aL}, l_L)^T$ and one $SU(2)$ singlet ν_s, the Lagrangian density is

$$\mathcal{L} = \mathcal{L}_{\rm SM} + \bar{\nu}_s i\partial\!\!\!/ \nu_s - Y\bar{L}_L\tilde{\Phi}\nu_{sR} + \text{H.c.} - M_s\overline{\nu_s}\nu_s, \tag{2.1}$$

where $\tilde{\Phi} = i\tau_2\Phi^*$ and Φ is the usual Higgs doublet. We consider temperatures sufficiently below the electroweak crossover at $T_{ew} \simeq 160$ GeV that the Higgs expectation value is very nearly the zero temperature value. After spontaneous symmetry breaking and in unitary gauge, the Yukawa coupling yields an off-diagonal Dirac mass term $m = Y\langle\Phi^0\rangle$ that mixes ν_s and ν_a, neglecting the Higgs active-sterile coupling, since we will focus solely on production via vector boson interactions, the Lagrangian density becomes

$$\mathcal{L} = \mathcal{L}_{\rm SM} + \bar{\nu}_s i\partial\!\!\!/ \nu_s - \bar{\nu}_\alpha \mathbb{M}_{\alpha\beta}\nu_\beta + \text{H.c.};$$
$$\alpha,\beta = a,s, \tag{2.2}$$

where a and s refer to active and sterile respectively and

$$\mathbb{M} = \begin{pmatrix} 0 & m \\ m & M_s \end{pmatrix}. \tag{2.3}$$

Introducing the "flavor" doublet (ν_a, ν_s), the diagonalization of the mass term $\mathbb{M}$ is achieved by a unitary transformation to the mass basis (ν_1, ν_2), namely,

$$\begin{pmatrix} \nu_a \\ \nu_s \end{pmatrix} = U(\theta)\begin{pmatrix} \nu_1 \\ \nu_2 \end{pmatrix};$$
$$U(\theta) = \begin{pmatrix} \cos(\theta) & \sin(\theta) \\ -\sin(\theta) & \cos(\theta) \end{pmatrix}, \tag{2.4}$$

where

$$\cos(2\theta) = \frac{M_s}{[M_s^2 + 4m^2]^{\frac{1}{2}}}; \qquad \sin(2\theta) = \frac{2m}{[M_s^2 + 4m^2]^{\frac{1}{2}}}. \tag{2.5}$$

In the mass basis,

$$\mathbb{M}_{diag} = U^{-1}(\theta)\mathbb{M}U(\theta) = \begin{pmatrix} M_1 & 0 \\ 0 & M_2 \end{pmatrix};$$
$$M_1 = \frac{1}{2}[M_s - [M_s^2 + 4m^2]^{\frac{1}{2}}];$$
$$M_2 = \frac{1}{2}[M_s + [M_s^2 + 4m^2]^{\frac{1}{2}}]. \tag{2.6}$$

We focus on the case $m \ll M_s$; therefore,

$$M_1 \simeq -\frac{m^2}{M_s}; \quad M_2 \simeq M_s; \quad \sin(2\theta) \simeq 2\theta \simeq \frac{2m}{M_s} \ll 1. \tag{2.7}$$

We refer to the heavier mass eigenstate with $M_2 \simeq M_s$ as *sterilelike* and the lighter mass eigenstate with $M_1 \propto m^2/M_s$ as *activelike*, since these are primarily composed of the sterile and active flavors in the flavor basis.

We work in unitary gauge which exhibits the physical degrees of freedom of massive vector bosons in thermodynamic equilibrium. The equations of motion were derived previously in Refs. [92–94]. In particular, Ref. [92] also includes contributions from Yukawa couplings between the sterile neutrino and scalar fields, but we will not consider such an extension here as this implies a particular model for the origin of the mass matrix. Our focus here is to study the sterile neutrino production solely from standard model interactions (charged and neutral currents) under the minimal set of assumptions discussed above.

Introducing the flavor doublet $\Psi^T = (\nu_a, \nu_s)$, the equation of motion *in the flavor basis* is [92–94] (for details, see the Appendix in Ref. [93])

$$(i\partial\!\!\!/\mathbb{1} - \mathbb{M} + \mathbf{\Sigma}'\mathbb{L})\Psi(\vec{x},t) + \int d^3x'dt'\mathbf{\Sigma}^r(\vec{x}-\vec{x}',t-t')\mathbb{L}\Psi(\vec{x}',t') = 0, \tag{2.8}$$

where $\mathbb{1}$ is the identity matrix in flavor space and $\mathbb{L} = (1-\gamma^5)/2$ is the left-handed chiral projection operator. The full one-particle irreducible self-energy includes local tadpole (Σ^t) and nonlocal dispersive ($\Sigma^r(\vec{x}-\vec{x}', t-t')$) contributions. It is solely arising from *standard model interactions to all orders* and is diagonal in the flavor basis, namely,

$$\mathbf{\Sigma} \equiv \Sigma \begin{pmatrix} 1 & 0 \\ 0 & 0 \end{pmatrix}. \tag{2.9}$$

Furthermore, in factoring out the projector $\mathbb{L}$, the remaining self-energy is calculated in the vectorlike theory. For example, the one-loop contributions to the self-energy are shown in Fig. 1; this is the leading order contribution to the self-energy.

Introducing the space-time Fourier transform in a spatial volume V,

$$\Psi(\vec{x}, t) = \frac{1}{\sqrt{V}} \sum_{\vec{q}} \int d\omega e^{i\vec{q}\cdot\vec{x}} e^{-i\omega t} \tilde{\Psi}(\omega, \vec{q}), \tag{2.10}$$

and similarly for the self-energy kernels, the effective Dirac equation in the flavor basis becomes [92–94] (see the Appendix in Ref. [93])

$$[(\gamma_0\omega - \vec{\gamma}\cdot\vec{q})\mathbb{1} - \mathbb{M} + (\mathbf{\Sigma}^t + \mathbf{\Sigma}(\omega, \vec{q}))\mathbb{L}]\tilde{\Psi}(\omega, \vec{q}) = 0; \tag{2.11}$$

this equation of motion is *exact*, since the self-energy includes all order contributions in standard model couplings. The bracket in (2.11) is the inverse or the retarded propagator of which the poles in the complex plane determine the dispersion relations and damping rates of *the mass eigenstates in the medium*.

The tadpole contribution $\mathbf{\Sigma}^t$, see Fig. 1(a) is local therefore it is independent of $\omega, \vec{q}$, in (2.11) $\Sigma(\omega, \vec{q})$, is the space-time Fourier transform of $\Sigma^r(\vec{x}-\vec{x}', t-t')$ and features a dispersive representation [92–94],

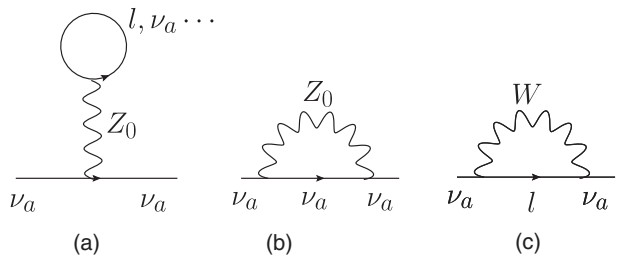

FIG. 1. One-loop contributions to the self-energy. The neutral current tadpole is proportional to the lepton (and quark) asymmetry.

$$\Sigma(\omega, \vec{q}) = \frac{1}{\pi}\int_{-\infty}^{\infty} dq_0 \frac{\mathrm{Im}\Sigma(q_0, \vec{q})}{q_0 - \omega - i0^+}. \tag{2.12}$$

From this dispersive form, it follows that

$$\Sigma(\omega, \vec{q}) = \mathrm{Re}\Sigma(\omega, \vec{q}) + i\mathrm{Im}\Sigma(\omega, \vec{q}) \tag{2.13}$$

with

$$\mathrm{Re}\Sigma(\omega, \vec{q}) = \frac{1}{\pi}\int_{-\infty}^{\infty} dq_0 \mathcal{P}\left[\frac{\mathrm{Im}\Sigma(q_0, \vec{q})}{q_0 - \omega}\right]. \tag{2.14}$$

The real part yields the "index of refraction" in the medium, and the imaginary part determines the *damping rate* of the single (quasi)particle excitations. The tadpole term must be calculated separately and does not feature a dispersive representation.

Although in this article we will focus on the one-loop contributions to the self-energy from standard model charged and neutral current interactions, the form of the equations of motion and the dispersive form of the self-energy (not the tadpole) are generally valid in principle to *all orders* in standard model interactions which are of the V–A form.

A subtle but important conceptual issue arises in the neutral current contribution to the self-energy with internal loop propagators for neutrinos. The propagators correspond to mass eigenstates; therefore, in principle, the perturbative loop expansion should be carried out in the *mass basis* rather than in the flavor basis. Furthermore, if the neutrino propagators describe neutrinos thermalized in the medium in terms of the equilibrium Fermi-Dirac distribution function, not only do these propagators correspond to mass (energy) eigenstates but are also *assumed* to be in thermal equilibrium. We will assume i) a very small mixing angle $\theta \ll 1$ so that to leading order in this mixing angle the activelike mass eigenstate can be taken to be the active flavor eigenstate and ii) in the temperature regime of interest in this article $T \simeq M_{W,Z}$, active (flavor) neutrinos are in (local) thermal equilibrium. Under these assumptions (the validity of which will be confirmed later), we consider the internal loop propagators in the neutral current contribution to be those of active neutrinos in thermal equilibrium to leading order in the mixing angle.

As a consequence of the V–A nature of the standard model couplings of neutrinos, $\Sigma(\omega, \vec{q})$ has the general form of a vectorlike theory,

$$\Sigma^t + \Sigma(\omega, \vec{q}) \equiv \gamma^0 A(\omega, \vec{q}) - \vec{\gamma}\cdot\hat{\mathbf{q}} B(\omega, \vec{q}), \tag{2.15}$$

and

$$\mathbf{\Sigma}^t + \mathbf{\Sigma}(\omega, \vec{q}) = \gamma^0 \mathbb{A}(\omega, \vec{q}) - \vec{\gamma}\cdot\hat{\mathbf{q}}\mathbb{B}(\omega, \vec{q}), \tag{2.16}$$

where in the flavor basis

$$\mathbb{A}(\omega,\vec{q})=\begin{pmatrix} A(\omega,\vec{q}) & 0 \\ 0 & 0 \end{pmatrix}; \quad \mathbb{B}(\omega,\vec{q})=\begin{pmatrix} B(\omega,\vec{q}) & 0 \\ 0 & 0 \end{pmatrix}. \tag{2.17}$$

The equations of motion simplify by projecting with $\mathbb{L}=(1-\gamma^5)/2; \mathbb{R}=(1+\gamma^5)/2$ and expanding in helicity eigenstates. Following the steps of Ref. [92], we write for the left (L) and right (R) fields

$$\Psi_L=\sum_{h=\pm 1} v^h \otimes \Psi^h_L; \qquad \Psi^h_L=\begin{pmatrix} \nu^h_a \\ \nu^h_s \end{pmatrix}_L \tag{2.18}$$

and

$$\Psi_R=\sum_{h=\pm 1} v^h \otimes \Psi^h_R; \qquad \Psi^h_R=\begin{pmatrix} \nu^h_a \\ \nu^h_s \end{pmatrix}_R, \tag{2.19}$$

where the left- and right-handed doublets are written in the *flavor* basis and v^h are eigenstates of the helicity operator

$$\hat{h}(\hat{\mathbf{q}})=\gamma^0\vec{\gamma}\cdot\hat{\mathbf{q}}\gamma^5=\vec{\sigma}\cdot\hat{\mathbf{q}}\begin{pmatrix} \mathbb{1} & 0 \\ 0 & \mathbb{1} \end{pmatrix}, \tag{2.20}$$

namely,

$$\vec{\sigma}\cdot\hat{\mathbf{q}}v^h=hv^h; \qquad h=\pm 1. \tag{2.21}$$

We find in the flavor basis the equation of motion for the left- and right-handed component doublets

$$[(\omega^2-q^2)\mathbb{1}+(\omega-hq)(\mathbb{A}+h\mathbb{B})-\mathbb{M}^2]\Psi^h_L=0 \tag{2.22}$$

and

$$[\omega-hq]\Psi^h_R=\mathbb{M}\gamma^0\Psi^h_L, \tag{2.23}$$

where $\mathbb{M}$ is given by (2.3) and

$$\mathbb{M}^2=\bar{M}^2\mathbb{1}+\frac{\delta M^2}{2}\begin{pmatrix} -\cos(2\theta) & \sin(2\theta) \\ \sin(2\theta) & \cos(2\theta) \end{pmatrix} \tag{2.24}$$

with

$$\bar{M}^2\equiv\frac{1}{2}(M_1^2+M_2^2); \qquad \delta M^2\equiv M_2^2-M_1^2, \tag{2.25}$$

and $M_{1,2}$ are given by Eq. (2.6). The results (2.22), (2.23) are *general* for standard model couplings of the active (flavor) neutrinos and sterile neutrinos that only interact with active ones via a seesaw-type mass matrix. Before discussing in detail the one-loop contribution from charged and neutral currents, we want to establish general results for the effective mixing angle in the medium and damping rates. The operator on the left-hand side of (2.22),

$$[\mathbb{S}^h_L(\omega,q)]^{-1}=[(\omega^2-q^2)\mathbb{1}+(\omega-hq)(\mathbb{A}+h\mathbb{B})-\mathbb{M}^2], \tag{2.26}$$

defines the inverse propagator in the flavor basis for the left-handed component projected on helicity eigenstates. The correct "mass eigenstates" correspond to the (complex) poles of $\mathbb{S}$, the real part describes the correct propagating frequencies, and the imaginary parts describe the damping rate of single (quasi)particle excitations. We will extract these mass eigenstates from the (complex) zeroes of $[\mathbb{S}^h_L]^{-1}$ by invoking the following approximations of which the validity will be assessed below:

(i) Ultrarelativistic approximation: $q\gg M_s$; this entails that the produced sterilelike neutrinos freeze out while relativistic.
(ii) $\theta\ll 1$; in particular we will assume that the self-energy correction is larger in magnitude than the vacuum mixing angle. The precise condition will be discussed below.
(iii) Validity of the perturbative expansion, in particular that the self-energy corrections, are smaller than the unperturbed dispersion relations. This assumption will be clarified and discussed in detail in the analysis that follows.

Introducing

$$\Omega^h\equiv(\omega-hq)(A(\omega,q)+hB(\omega,q)) \tag{2.27}$$

and using (2.24), we obtain

$$[\mathbb{S}^h_L(\omega,q)]^{-1}=\left(\omega^2-q^2-\bar{M}^2+\frac{\Omega^h}{2}\right)\mathbb{1}-\frac{1}{2}\sqrt{(\delta M^2\cos(2\theta)+\Omega^h)^2+(\delta M^2\sin(2\theta))^2}\begin{pmatrix} -\mathbb{C}^h_m(\omega,q) & \mathbb{S}^h_m(\omega,q) \\ \mathbb{S}^h_m(\omega,q) & \mathbb{C}^h_m(\omega,q) \end{pmatrix}, \tag{2.28}$$

where

$$\mathbb{C}^h_m(\omega,q)=\frac{\delta M^2\cos(2\theta)+\Omega^h(\omega,q)}{\sqrt{(\Omega^h(\omega,q)+\delta M^2\cos(2\theta))^2+(\delta M^2\sin(2\theta))^2}} \tag{2.29}$$

$$\mathbb{S}^h_m(\omega,q) = \frac{\delta M^2\sin(2\theta)}{\sqrt{(\Omega^h(\omega,q)+\delta M^2\cos(2\theta))^2+(\delta M^2\sin(2\theta))^2}}, \tag{2.30}$$

with

$$(\mathbb{C}^h_m(\omega,q))^2+(\mathbb{S}^h_m(\omega,q))^2=1. \tag{2.31}$$

If the imaginary part of the self-energy vanishes (or can be neglected), then

$$\mathbb{C}^h_m(\omega,q)=\cos(2\theta_m);\qquad \mathbb{S}^h_m(\omega,q)=\sin(2\theta_m), \tag{2.32}$$

and θ_m would be the mixing angle in the medium. However, the absorptive (imaginary) part of the self-energy (related to the damping rate of quasiparticle excitations) prevent such identification.

The matrix

$$\begin{pmatrix} -\mathbb{C}^h_m(\omega,q) & \mathbb{S}^h_m(\omega,q)\\ \mathbb{S}^h_m(\omega,q) & \mathbb{C}^h_m(\omega,q)\end{pmatrix}$$

has null trace and determinant (-1) as a consequence of (2.31); therefore, *real* eigenvalues $\lambda=\pm1$ with the following eigenvectors,

$$\begin{pmatrix} c^h(\omega,q)\\ -s^h(\omega,q)\end{pmatrix};\qquad \lambda=-1 \tag{2.33}$$

$$\begin{pmatrix} s^h(\omega,q)\\ c^h(\omega,q)\end{pmatrix};\qquad \lambda=1, \tag{2.34}$$

where

$$c^h(\omega,q)=\left[\frac{1+\mathbb{C}^h_m(\omega,q)}{2}\right]^{1/2} \tag{2.35}$$

$$s^h(\omega,q)=\left[\frac{1-\mathbb{C}^h_m(\omega,q)}{2}\right]^{1/2}. \tag{2.36}$$

For vanishing absorptive part $s^h\equiv\sin(\theta_m)$, $c^h\equiv\cos(\theta_m)$ with θ_m the (real) mixing angle in the medium.

To leading order for $\theta\ll1$ and $M_1\ll M_2\simeq M_s$ we obtain the following eigenvalues of $[\mathbb{S}]^{-1}$:

$$S^{-1}\simeq\omega^2-q^2-M_2^2-\frac{\theta^2(M_2^2)^2}{(M_2^2+\Omega^h(\omega,q))}+\theta^2M_2^2;$$

$$\text{for } \lambda=+1;\qquad \text{eigenvector}\quad \begin{pmatrix} s^h(\omega,q)\\ c^h(\omega,q)\end{pmatrix} \tag{2.37}$$

$$S^{-1}\simeq\omega^2-q^2-M_1^2+\Omega^h(\omega,q)+\frac{\theta^2(M_2^2)^2}{(M_2^2+\Omega^h(\omega,q))}-\theta^2M_2^2;$$

$$\text{for } \lambda=-1;\qquad \text{eigenvector}\quad \begin{pmatrix} c^h(\omega,q)\\ -s^h(\omega,q)\end{pmatrix}. \tag{2.38}$$

It is clear that the eigenvector corresponding to eigenvalue $+1$ corresponds to a sterilelike neutrino in the medium; the radiative correction (self-energy) enters solely with the mixing angle and vanishes for vanishing mixing angle, whereas the eigenvector corresponding to eigenvalue -1 is activelike, with radiative correction (Ω^h) even for $\theta=0$. The inverse of $[\mathbb{S}^h_L(\omega,q)]^{-1}$ is the inverse of the propagator, and therefore its complex zeroes describe the complex poles. Under the assumption of the validity of perturbation theory (discussed below in detail), we write

$$\omega=\omega_j(q)+\delta\omega^h_j;\qquad \omega_j(q)=\sqrt{q^2+M_j^2}\simeq q+\frac{M_j^2}{2q};\qquad j=1,2 \tag{2.39}$$

in the relativistic approximation and introducing (in the relativistic limit)

$$\Delta^h_j(q)+i\gamma^h_j(q)=\frac{\Omega^h(\omega_j,q)}{2q}\simeq\frac{(\omega_j-hq)}{2q}[A(\omega=q,q)+hB(\omega=q,q)], \tag{2.40}$$

with $j=2$ for sterilelike (eigenvalue $\lambda=1$) and $j=1$ for activelike (eigenvalue $\lambda=-1$) where both Δ and γ are real, and introducing

$$\xi=\frac{M_s^2}{2q} \tag{2.41}$$

we find the position of the poles in the propagator (mass eigenstates) at

$$\delta\omega^h_2=\frac{\theta^2(\xi+\Delta^h_2(q)-i\gamma^h_2(q))}{[(1+\frac{\Delta^h_2(q)}{\xi})^2+(\frac{\gamma^h_2(q)}{\xi})^2]}-\theta^2\xi;$$

$$\text{for } \lambda=+1;\qquad \text{eigenvector}\quad \begin{pmatrix} s^h(\omega=q,q)\\ c^h(\omega=q,q)\end{pmatrix} \tag{2.42}$$

for the "sterilelike" neutrino and

$$\delta\omega_1^h = -(\Delta_1^h(q) + i\gamma_1^h(q)) - \frac{\theta^2(\xi + \Delta_1^h(q) - i\gamma_1^h(q))}{[(1+\frac{\Delta_1^h(q)}{\xi})^2 + (\frac{\gamma_1^h(q)}{\xi})^2]} + \theta^2\xi;$$

$$\text{for } \lambda = -1; \quad \text{eigenvector} \quad \begin{pmatrix} c^h(\omega = q, q) \\ -s^h(\omega = q, q) \end{pmatrix} \tag{2.43}$$

for the "activelike" neutrino.

We now introduce the *effective mixing angle in the medium*,

$$\theta^h_{\rm eff}(q) = \frac{\theta}{[(1+\frac{\Delta_j^h(q)}{\xi})^2 + (\frac{\gamma_j^h(q)}{\xi})^2]^{1/2}}, \tag{2.44}$$

for each mass eigenstate $j = 1, 2$, in terms of which the position of the (quasi)particle poles (2.42), (2.43) are written as

$$\delta\omega_2^h = \Delta_2^h(q)(\theta^h_{\rm eff}(q))^2 + \xi[(\theta^h_{\rm eff}(q))^2 - \theta^2] - i\gamma_2^h(q)(\theta^h_{\rm eff}(q))^2; \quad j = 2 \quad \text{(sterilelike)}, \tag{2.45}$$

$$\delta\omega_1^h = -\Delta_1^h(q)[1 + (\theta^h_{\rm eff}(q))^2] - \xi[(\theta^h_{\rm eff}(q))^2 - \theta^2] - i\gamma_1^h(q)[1 - (\theta^h_{\rm eff}(q))^2]; \quad j = 1 \quad \text{(activelike)}. \tag{2.46}$$

Writing

$$\delta\omega_j^h = \Delta E_j^h - i\frac{\Gamma_j^h}{2}, \tag{2.47}$$

for the corresponding helicity component, the imaginary part Γ yields the damping rate for the single (quasi)particle excitations in the medium; namely, the mass eigenstates in the medium evolve in time as

$$\nu_j^h(q) \simeq e^{-i\omega_j t}e^{-i\Delta E_j^h t}e^{-\Gamma_j^h t/2} \Rightarrow |\nu_j^h(q)|^2 \simeq e^{-\Gamma_j^h t}; \quad j = 1, 2, \tag{2.48}$$

where the damping rates Γ_j^h are given by

$$\Gamma_2^h = 2\gamma^h(q)(\theta^h_{\rm eff}(q))^2 \simeq 2\gamma^h(q)\sin^2(\theta^h_{\rm eff}) \quad \text{sterilelike} \tag{2.49}$$

$$\Gamma_1^h = 2\gamma^h(q)[1 - (\theta^h_{\rm eff}(q))^2] \simeq 2\gamma^h(q)\cos^2(\theta^h_{\rm eff}) \quad \text{activelike}. \tag{2.50}$$

Even when a particle cannot decay in the vacuum, the spectral density may feature a width in the medium as a consequence of dissipative processes arising from the coupling to excitations in the medium. In this case, the width describes the relaxation of the quasiparticle in the linear response [95–98].

The coefficient ω–hq in (2.27) is noteworthy: for positive ω, the positive helicity component $h = 1$ is *helicity* suppressed, on the mass shell of the (vacuum) mass eigenstates in the relativistic limit $\omega - q \simeq M_{1,2}^2/2q$. This is the usual helicity suppression from the V–A form of the interaction and has important consequences: the damping rate for *positive helicity* sterilelike neutrinos is much smaller than that for the negative helicity, and the medium corrections to the mixing angle are also *suppressed* for the positive helicity component. This suppression will have important and unexpected consequences on the rate of production of the sterilelike species as will be discussed below in detail.

The functions $\gamma^{\pm}(q)$ require the combinations $A \mp B$ that define the self-energy (2.15); these combinations are handily extracted as follows: introducing the 4-vectors

$$Q_\mu^- = \frac{1}{q}(q, -\vec{q}); \qquad Q_\mu^+ = \frac{1}{q}(q, \vec{q}) \tag{2.51}$$

and defining

$$\Sigma^-(q) \equiv A(\omega = q, q) - B(\omega = q, q); \quad \Sigma^+(q) \equiv A(\omega = q, q) + B(\omega = q, q), \tag{2.52}$$

we obtain

$$(A(\omega, q) - B(\omega, q))_{\omega=q} = \frac{1}{4}{\rm Tr}\not{Q}^-\Sigma(q, q) \equiv \Sigma^-(q), \tag{2.53}$$

$$(A(\omega, q) + B(\omega, q))_{\omega=q} = \frac{1}{4}{\rm Tr}\not{Q}^+\Sigma(q, q) \equiv \Sigma^+(q), \tag{2.54}$$

$$\gamma^-(q) = {\rm Im}\Sigma^-(q) \quad \text{(negative helicity)} \tag{2.55}$$

$$\gamma^+(q) = \left[\frac{M_s}{2q}\right]^2 {\rm Im}\Sigma^+(q) \quad \text{(positive helicity)} \tag{2.56}$$

$$\Delta^-(q) = {\rm Re}\Sigma^-(q) \quad \text{(negative helicity)} \tag{2.57}$$

$$\Delta^+(q) = \left[\frac{M_s}{2q}\right]^2 {\rm Re}\Sigma^+(q) \quad \text{(positive helicity)}. \tag{2.58}$$

The damping rates for negative (−) and positive (+) sterilelike neutrinos respectively are given by

$$\Gamma_2^{\mp}(q) = 2(\theta^{\mp}_{\rm eff}(q))^2\gamma^{\mp}(q); \tag{2.59}$$

as discussed in the next section, these rates determine the production rates of sterile neutrinos of each helicity. For the activelike neutrinos, we find

$$\Gamma_1^-(q) = 2[1-(\theta_{\rm eff}^-(q))^2]{\rm Im}\Sigma^-(q) \tag{2.60}$$

$$\Gamma_1^+(q) = 2[1-(\theta_{\rm eff}^-(q))^2]\left[\frac{M_1}{2q}\right]^2{\rm Im}\Sigma^+(q) \tag{2.61}$$

for negative $(-)$ and positive $(+)$ helicity respectively, and the latter rate can be safely neglected for the light activelike neutrinos. The effective mixing angles are given by

$$\theta_{\rm eff}^{\pm}(q) = \frac{\theta}{[(1+\frac{\Delta^{\pm}(q)}{\xi})^2+(\frac{\gamma^{\pm}(q)}{\xi})^2]^{1/2}}, \tag{2.62}$$

where in the relativistic limit

$$\frac{\Delta^-(q)}{\xi} = \frac{2q}{M_s^2}{\rm Re}\Sigma^-(q);$$
$$\frac{\Delta^+(q)}{\xi} = \frac{{\rm Re}\Sigma^+(q)}{2q} \tag{2.63}$$

$$\frac{\gamma^-(q)}{\xi} = \frac{2q}{M_s^2}{\rm Im}\Sigma^-(q);$$
$$\frac{\gamma^+(q)}{\xi} = \frac{{\rm Im}\Sigma^+(q)}{2q}, \tag{2.64}$$

where $\Sigma^{\pm}$ are given by (2.53), (2.54).

The important observation is that the self-energy $\Sigma(\omega,q)$ is calculated in the *standard model for massless flavor neutrinos*.

The result for the effective mixing angle (2.62) is valid for $\theta \ll 1$, and (2.63), (2.64) are valid in the relativistic limit $q \gg M_s$ but are otherwise general and *valid to all orders in perturbation theory in standard model couplings*.

A MSW [90] resonance is available whenever

$$\frac{\Delta^{\pm}(q)}{\xi} = -1, \tag{2.65}$$

for $\cos(\theta) \simeq 1$. However, this resonance is *screened* by the imaginary part (damping rate) (this phenomenon was also noticed in Ref. [26]), and under the condition that $\theta \ll 1$ and the validity of the approximations leading to the above results, the possible presence of this resonance will not yield a large enhancement in the effective mixing angle. This aspect will be discussed in detail in Sec. IV.

These expressions are one of the main results of this study and summarize the effective mixing angles and damping rates *generically* for standard model interactions under the assumptions of the validity of the relativistic approximation, perturbative expansion and $\theta \ll 1$.

From the expressions (2.29), (2.30) and (2.35), (2.36), one finds that for $\theta \ll 1$

$$s^h(\omega = q, q) \simeq \theta_{\rm eff}^h(q)e^{-i\phi^h(q)};$$
$$\phi^h(q) = \tan^{-1}\left[\frac{\gamma^h(q)}{\xi+\Delta^h(q)}\right], \tag{2.66}$$

where the phase is irrelevant for transition probabilities and the quantum kinetic description of sterile neutrino production because the relevant quantity is the transition probability per unit time.

III. QUANTUM KINETICS: PRODUCTION RATES

In order to understand how to extract the rate of sterilelike neutrino production from the damping rate obtained from the self-energy and the effective mixing angle in the medium, let us consider first the quantum kinetics of production of the sterilelike mass eigenstate from W-decay in the case of the vacuum mixing angle. This analysis clearly shows how the mixing angle in the medium enters in the quantum kinetic equation with a straightforward generalization to more general production processes.

If the mass M_2 of the heavy, sterilelike neutrino is such that $M_W > M_2 + m_l$ with m_l the mass of the charged lepton l, then the mass eigenstate corresponding to the sterilelike neutrino can be produced from W-decay, and a similar argument applies to Z-decay if $M_Z > M_2 + M_1$. The charged current interaction vertex for the case of one generation is

$$\mathcal{L}_{cc} = \frac{g_w}{\sqrt{2}}[\bar{l}\gamma^\mu \mathbb{L}\nu_l W_\mu + {\rm H.c.}]. \tag{3.1}$$

Writing the flavor eigenstate ν_l in the mass basis as

$$\nu_l = \cos(\theta)\nu_1 + \sin(\theta)\nu_2 \tag{3.2}$$

with ν_1 being the activelike and ν_2 being the sterilelike mass eigenstates with M_1 and M_2 respectively, yielding an interaction vertex for the sterilelike mass eigenstate ν_2,

$$\mathcal{L}_{s,cc} = \frac{g_w}{\sqrt{2}}\sin(\theta)[\bar{l}\gamma^\mu \mathbb{L}\nu_2 W_\mu + {\rm H.c.}]. \tag{3.3}$$

The dynamics of the production of ν_2 from the process $W \to \bar{l}\nu_2$ is obtained via the quantum kinetic equation for the process $W \rightleftharpoons \bar{l}\nu_2$[89], namely,

$$\frac{dn_2(q;t)}{dt} = \left.\frac{dn_2(q;t)}{dt}\right|_{\rm gain} - \left.\frac{dn_2(q;t)}{dt}\right|_{\rm loss}, \tag{3.4}$$

where $n_2(q;t)$ is the distribution function of the sterilelike mass eigenstate ν_2 and the gain and loss terms are extracted from the usual transition probabilities per unit time,

$$\left.\frac{dn_2(q;t)}{dt}\right|_{\rm gain} = \frac{2\pi\sin^2(\theta)}{2E_2(q)}\int\frac{d^3k|\mathcal{M}_{fi}|^2}{(2\pi)^3 2E_W(p)2E_l(k)}N_B(p)(1-n_l(k))(1-n_2(q;t))\delta(E_W(p)-E_l(k)-E_2(q))$$
$$\left.\frac{dn_2(q;t)}{dt}\right|_{\rm loss} = \frac{2\pi\sin^2(\theta)}{2E_2(q)}\int\frac{d^3k|\mathcal{M}_{fi}|^2}{(2\pi)^3 2E_W(p)2E_l(k)}(1+N_B(p))n_l(k)n_2(q;t)\delta(E_W(p)-E_l(k)-E_2(q)), \tag{3.5}$$

where $p=|\vec{k}+\vec{q}|$ and

$$N_B(p)=\frac{1}{e^{E_W(p)/T}-1}; \qquad n_l(k)=\frac{1}{e^{E_l(k)/T}+1}, \tag{3.6}$$

and $|\mathcal{M}_{fi}|^2$ is the usual transition matrix element for $W\to\bar{l}\nu$ and we have assumed that the W vector boson and charged lepton l are in thermal equilibrium and have displayed explicitly the factor $\sin^2(\theta)$ factored out of the M_{fi}. Therefore, the quantum kinetic equation (3.4) becomes of the form

$$\frac{dn_2(q;t)}{dt}=\Gamma^{<}(q)(1-n_2(q;t))-\Gamma^{>}(q)n_2(q;t), \tag{3.7}$$

where the gain and loss *rates* are

$$\Gamma^{<}(q)=\frac{2\pi\sin^2(\theta)}{2E_2(q)}\int\frac{d^3k|\mathcal{M}_{fi}|^2}{(2\pi)^3 2E_W(p)2E_l(k)}N_B(p) \times(1-n_l(k))\delta(E_W(p)-E_l(k)-E_2(q)) \tag{3.8}$$

$$\Gamma^{>}(q)=\frac{2\pi\sin^2(\theta)}{2E_2(q)}\int\frac{d^3k|\mathcal{M}_{fi}|^2}{(2\pi)^3 2E_W(p)2E_l(k)} \times(1+N_B(p))n_l(k)\delta(E_W(p)-E_l(k)-E_2(q)). \tag{3.9}$$

Because the W, l_α are in thermal equilibrium, the gain and loss rates obey the *detailed balance condition*

$$\Gamma^{<}(q)e^{E_2(q)/T}=\Gamma^{>}(q), \tag{3.10}$$

which can be confirmed straightforwardly from the explicit expressions (3.8), (3.9) using the energy conserving delta functions and the relations

$$1+N_B(E)=e^{E/T}N_B(E);$$
$$1-n_l(E)=e^{E/T}n_l(E). \tag{3.11}$$

Using (3.10), the quantum kinetic equation (3.7) reads

$$\frac{dn_2(q;t)}{dt}=\Gamma_2(q)[n_{eq}(q)-n_2(q;t)], \tag{3.12}$$

where

$$n_{eq}(q)=\frac{1}{e^{\frac{E_2(q)}{T}}+1} \tag{3.13}$$

is the *equilibrium* (Fermi-Dirac) distribution function and

$$\Gamma_2(q)=\Gamma^{>}(q)+\Gamma^{<}(q) =\frac{2\pi\sin^2(\theta)}{2E_2(q)}\int\frac{d^3k|\mathcal{M}_{fi}|^2}{(2\pi)^3 2E_W(p)2E_l(k)} \times[N_B(p)+n_l(k)]\delta(E_W(p)-E_l(k)-E_2(q)). \tag{3.14}$$

The approach to equilibrium is studied by writing $n_2(q;t)=n_{eq}(q)+\delta n_2(q;t)$; it follows from (3.7) that

$$\delta n_2(q;t)=\delta n_2(q;0)e^{-\Gamma_2(q)t}. \tag{3.15}$$

The relaxation rate $\Gamma_2(q)$ is precisely the damping rate of single (quasi)particle excitations (2.48) as discussed in Refs. [95–98]. Neutral current interactions are treated similarly by passing to the mass basis and keeping only the linear term in $\sin(\theta)\simeq\theta$ for $\theta\ll 1$. It is clear from (3.14) that

$$\Gamma_2(q)=\sin^2(\theta)\Gamma_{sm}(q), \tag{3.16}$$

where $\Gamma_{sm}(q)$ is the rate calculated in the standard model for the production of a massive neutrino; furthermore, it is given by the *imaginary part of the standard model flavor neutrino self-energy* evaluated on the massive neutrino mass shell. In the limit of a relativistic sterilelike mass eigenstate, $\Gamma_{sm}(q)$ is *identical* to the imaginary part of the self-energy for an active massless neutrino in the standard model. In fact, in this limit, the quantum kinetic equation for the activelike mass eigenstate in the relativistic limit is the same as (3.12) but with $\sin^2(\theta)$ in (3.16) replaced by $\cos^2(\theta)$.

Fundamentally, the heart of the argument is simply detailed balance, a consequence of the main assumption that the plasma degrees of freedom are in thermodynamic equilibrium; the damping rate of single quasiparticle excitations $\Gamma_2(q)$ determines the approach to equilibrium in linear response [95–98], and for $\theta\ll 1$, the quantum kinetic equation is linear in the population n_2 to leading order in θ. Therefore, the gain term in the quantum kinetic equation is simply related to the relaxation rate by detailed

balance. This argument is general for $\theta \ll 1$. Therefore, comparing with the damping rate for the sterilelike mass eigenstate (2.49), this analysis makes it clear that for $\theta \ll 1$ the medium effects on the mixing angle in the quantum kinetic equation are incorporated by the simple replacement $\sin(\theta) \to \theta_{\rm eff}(q)$ in (3.14), (3.16); in other words, the *full quantum kinetic equation for sterilelike production* is

$$\frac{dn_2^h(q;t)}{dt} = \Gamma_2^h(q)[n_{eq}(q) - n_2^h(q;t)], \qquad (3.17)$$

where $\Gamma_2^{\mp}(q)$ are given by (2.59) with (2.55) and (2.55). Hence, the *production* rate of sterilelike neutrinos is

$$\Gamma^h_{\rm prod}(q) = \Gamma_2^h(q) n_{eq}(q). \qquad (3.18)$$

In summary, the production rates for sterilelike neutrinos of negative (−) and positive (+) helicities are given by

$$\Gamma^-_{\rm prod}(q) = 2(\theta^-_{\rm eff}(q))^2 {\rm Im}\Sigma^-(q) n_{eq}(q) \qquad (3.19)$$

$$\Gamma^+_{\rm prod}(q) = 2(\theta^+_{\rm eff}(q))^2 \left[\frac{M_s}{2q}\right]^2 {\rm Im}\Sigma^+(q) n_{eq}(q), \qquad (3.20)$$

where the mixing angles $\theta^{\mp}_{\rm eff}(q)$ are given by (2.44) with the definitions (2.55)–(2.58). In the production rates (3.19), (3.20), $\Sigma(q)$ is the *standard model self-energy for flavor neutrinos* evaluated on the relativistic mass shell, and n_2^h refer to the population of the *sterilelike mass eigenstate* of helicity h. Because $\theta_{\rm eff}$ depends on helicity, the matrix elements M_{fi} *should not* be averaged over helicity (spin) states.

Expression (3.14), also shows how the helicity suppression is manifest in the case of massive neutrinos. To understand this aspect, it is convenient to look at the positive frequency solutions of the massive Dirac equation in the chiral representation ($\gamma^5 = {\rm diag}(\mathbb{1}, -\mathbb{1})$) and in the helicity basis,

$$\mathcal{U}_+(\vec{q}) = N\begin{pmatrix} v_+(\vec{q}) \\ -\varepsilon(q) v_+(\vec{q}) \end{pmatrix};$$
$$\mathcal{U}_-(\vec{q}) = N\begin{pmatrix} -\varepsilon(q) v_-(\vec{q}) \\ v_-(\vec{q}) \end{pmatrix}, \qquad (3.21)$$

where $v_\pm(\vec{q})$ are helicity eigenvectors (Weyl spinors) for $h = \pm 1$ and

$$N = \sqrt{E_s(q) + q}; \qquad \varepsilon(q) = \frac{M_s}{E(q) + q}, \qquad (3.22)$$

then

$$\mathbb{L}\mathcal{U}_+(\vec{q}) = \varepsilon(q) N \begin{pmatrix} 0 \\ v_+(\vec{q}) \end{pmatrix} \qquad (3.23)$$

in the relativistic limit $q \gg M_s$, $\varepsilon \simeq M_s/2q$, this projected wave function enters in the matrix element M_{fi} for a massive positive helicity neutrino in the final state, therefore

$$|M_{fi}|^2 \propto \left(\frac{M_s}{2q}\right)^2 \qquad (3.24)$$

in agreement with the helicity suppression for the damping rate discussed in the previous section.

A. Generality

Although in the above discussion we focused on the production process $W \to \bar{l}\nu_2$, the result (3.17) is general for $\theta \ll 1$. Consider the standard model charged and neutral current vertices. Writing these in the basis of mass eigenstates, the charged current vertex is linear in the mass eigenstate ν_2, and therefore the vertex is $\propto \theta$. The neutral current vertex would feature a term linear in θ ($\propto \bar{\nu}_1\nu_2$) and another $\propto \theta^2$ ($\propto \bar{\nu}_2\nu_2$); for $\theta \ll 1$, this last term can be neglected, and both charged and neutral current vertices are *linear* in θ and ν_2. Furthermore, $\theta \ll 1$ justifies taking the activelike mass eigenstate to be in LTE in the medium for $T \geq 0.1$ MeV as its relaxation rate is much larger than that of the sterilelike eigenstate which is suppressed by $\propto \theta^2 \ll 1$. Because the interaction vertices are linear in the neutrino field to leading order in θ, the quantum kinetic equation (gain-loss) is obviously of the form (3.7), and because the degrees of freedom that lead to the gain and loss terms are all in LTE, the gain ($\Gamma^<$) and loss ($\Gamma^>$) rates must obey the detailed balance condition (3.10). This analysis yields the directly to the quantum kinetic equation (3.12) after replacing $\theta \to \theta_{\rm eff}(q)$ where q is the momentum of the sterile-like neutrino on its mass shell, the $|M_{fi}|^2$ matrix element for the gain and loss transition rates are insensitive to the phase in (2.66). Analyzing the approach to equilibrium leads to the identification of Γ_2 with the damping rate of the sterilelike mass eigenstate. This argument is general, and the analysis presented above for $W \to \bar{l}\nu_2$ provides a direct example, which will be the focus of a detailed analysis in the next section.

IV. STERILE PRODUCTION FROM VECTOR BOSON DECAY

We now consider the description of sterile(like) neutrino production via vector boson decay $W \to \bar{l}\nu_2; Z^0 \to \bar{\nu}_1\nu_2$ at temperature $T \simeq M_{w,z}$, this is the leading order production process at this temperature. This temperature scale is sufficiently lower than the electroweak crossover scale $T \simeq 160$ GeV so that the Higgs field is near its vacuum expectation value and the finite temperature corrections to the W, Z masses can be safely neglected [25]. At high temperature, the propagator of charged leptons receives substantial hard thermal loop corrections

from electromagnetic interactions (and quarks from both photons and gluons) for momenta $\leq eT$ [98–102]. However, the decay of a vector boson *at rest* in the plasma yields particles with momenta $\simeq M_{W,Z}/2$; therefore, the typical momenta of the charged lepton is $\mathcal{O}(T)$, and in this regime, the hard thermal loop corrections are subleading and will be neglected in the following analysis. For the same reason, a sterile neutrino of mass $M_2 \ll M_{W,Z}$ will be produced relativistically. Low momentum sterile neutrinos (and charged leptons) *can* be produced for highly boosted vector bosons in the medium, but those excitations will be Boltzmann suppressed for $T \simeq M_{W,Z}$, and this will be explicitly confirmed in the analysis below.

We will take the charged lepton and the activelike neutrino to be massless and refer generically to the vector boson mass as M, adapting the general result to the W, Z *a posteriori*. Under this approximation (justified for $M_2 \ll T \simeq M_{W,Z}$), the one-loop self-energy is the same for both charged and neutral current interactions; in the latter case, the loop in Fig. 1(b) includes the activelike neutrino (self-consistently) assumed to be in LTE.

The one-loop tadpole contribution from neutral currents Fig. 1 is given by [92,103]

$$\Sigma^t = -\gamma^0 \pi \frac{\alpha_w}{M_W^2} \sum_f C_v^{(f)} \int \frac{d^3k}{(2\pi)^3} [n_f(k) - \bar{n}_f(k)]$$
$$= -\gamma^0 \frac{\pi}{6} \alpha_w \left(\frac{T}{M_w}\right)^2 \sum_f C_v^{(f)} \mu^f \left[1 + \frac{\mu_f^2}{\pi^2 T^2}\right], \tag{4.1}$$

where f are all the ultrarelativistic fermionic species in thermal equilibrium at temperature T and chemical equilibria with chemical potentials μ^f respectively. The tadpole Σ^t is independent of frequency and momentum and contributes only to A in (2.15) and (2.17). Although we quote this result as part of the general formulation, we will neglect the lepton and quark asymmetries in the following analysis, setting $\mu^f = 0$ for all fermionic species, thereby neglecting the contribution Σ^t to the self-energy.

We obtain the imaginary part of the self-energy (for both helicities) in (2.13), from which we will obtain the real part from the dispersion relation (2.14).

For both charged and neutral current contributions [Figs. 1(b) and 1(c)] for relativistic leptons, the imaginary part of the self-energy is given by [92]

$$Im\Sigma(q_0, \vec{q}) = \pi g^2 \int \frac{d^3k}{(2\pi)^3} \int_{-\infty}^{\infty} dk_0 [1 - n_f(k_0) + N_b(p_0)] \gamma^\mu$$
$$\times \rho_f(k_0, \vec{k}) \rho_b(p_0, \vec{p}) \gamma^\nu P_{\mu\nu}(p_0, \vec{p});$$
$$p^\mu = q^\mu - k^\mu, \tag{4.2}$$

where f stands for the fermionic species, either a charged lepton l for the charged current or the active neutrino ν_a (assumed in thermal equilibrium) for the neutral current contributions and b for either vector boson in the intermediate state. The couplings and masses for the charged and neutral current contributions are

$$g = \begin{cases} \frac{g_w}{\sqrt{2}} & \text{CC} \\ \frac{g_w}{2\cos(\theta_w)} & \text{NC} \end{cases};$$
$$M = \begin{cases} M_W & \text{CC} \\ M_Z = \frac{M_W}{\cos(\theta_w)} & \text{NC} \end{cases};$$
$$\sin^2(\theta_w) \simeq 0.23; \qquad \alpha_w = \frac{g_w^2}{4\pi} \simeq \frac{1}{32}. \tag{4.3}$$

The spectral densities ρ_f, ρ_b are respectively (for massless fermions)

$$\rho_f(k_0, \vec{k}) = \frac{\not{k}}{2k} [\delta(k_0 - k) - \delta(k_0 + k)];$$
$$\not{k} = \gamma^0 k^0 - \vec{\gamma} \cdot \vec{k}, \tag{4.4}$$

$$\rho_b(p_0, \vec{p}) = \frac{1}{2W_p} [\delta(p^0 - W_p) - \delta(p^0 + W_p)];$$
$$W_p = \sqrt{p^2 + M^2}; \qquad p^\mu = q^\mu - k^\mu, \tag{4.5}$$

and the projection operator

$$P_{\mu\nu}(p_0, \vec{p}) = -\left[g_{\mu\nu} - \frac{p_\mu p_\nu}{M^2}\right]; \qquad p^\mu = (p^0, \vec{p});$$
$$M^2 \equiv M_{z,w}^2 \tag{4.6}$$

and

$$n_f(k_0) = \frac{1}{e^{k_0/T} + 1}; \qquad N_b(p_0) = \frac{1}{e^{p_0/T} - 1}. \tag{4.7}$$

As per the discussion in the previous sections [see Eqs. (2.27) and (2.40)], we need the combinations $A(q_0, q) \pm B(q_0, q)$ which are obtained from the traces (2.53), (2.54). We find

$$\text{Im}[A(q_0, q) \mp B(q_0, q)]$$
$$= \pi g^2 \int_{-\infty}^{\infty} dk_0 \int \frac{d^3k}{(2\pi)^3 4kW_p} L^{\mu\nu}[Q^\pm; k] P_{\mu\nu}[p] \bar{\rho}_f$$
$$\times (k_0, k) \bar{\rho}_b(p_0, p) [1 - n_f(k_0) + N_b(p_0)], \tag{4.8}$$

where

$$\bar{\rho}_f(k_0, k) = [\delta(k_0 - k) - \delta(k_0 + k)] \tag{4.9}$$

$$\bar{\rho}_b(p_0,p) = [\delta(p_0 - W_p) - \delta(p_0 + W_p)]; \quad p^\mu = q^\mu - k^\mu \tag{4.10}$$

and

$$L^{\mu\nu}[Q;k] = [Q^\mu k^\nu + Q^\nu k^\mu - g^{\mu\nu} Q\cdot k]. \tag{4.11}$$

Using the various delta functions from $\bar{\rho}_f;\bar{\rho}_b$ we find for the negative helicity component

$$L^{\mu\nu}[Q^+,k]P_{\mu\nu}[p] = -\frac{M^2}{q}[F_1(q_0,q) + k^0 F_2(q_0,q)], \tag{4.12}$$

with

$$F_1(q_0,q) = \left[1 - \left(\frac{(q^0)^2 - q^2}{M^2}\right)\right]\left[1 - \frac{(q^0-q)^2}{2M^2}\right] \tag{4.13}$$

$$F_2(q_0,q) = 2\frac{(q^0-q)}{M^2}\left[1 - \left(\frac{(q^0)^2 - q^2}{2M^2}\right)\right]. \tag{4.14}$$

Similarly, for the positive helicity component,

$$L^{\mu\nu}[Q^-,k]P_{\mu\nu}[p] = \frac{M^2}{q}[G_1(q_0,q) + k^0 G_2(q_0,q)], \tag{4.15}$$

with

$$G_1(q_0,q) = \left[1 - \left(\frac{(q^0)^2 - q^2}{M^2}\right)\right]\left[1 - \frac{(q^0+q)^2}{2M^2}\right] \tag{4.16}$$

$$G_2(q_0,q) = 2\frac{(q^0+q)}{M^2}\left[1 - \left(\frac{(q^0)^2 - q^2}{2M^2}\right)\right]. \tag{4.17}$$

Note the relation

$$G_1(q^0,q) = F_1(q^0,-q); \qquad G_2(q^0,q) = F_2(q^0,-q). \tag{4.18}$$

Using the results above, it is straightforward to show that

$$\mathrm{Im}[A(q_0,q) + B(q_0,q)] = \mathrm{Im}[A(-q_0,q) - B(-q_0,q)]. \tag{4.19}$$

This identity relates the imaginary parts for positive energy, negative helicity neutrinos to negative energy positive helicity (antineutrinos) (in the absence of a chemical potential). This identity guarantees that the production rate for negative (positive) helicity neutrinos is the same as for positive (negative) helicity antineutrinos and is a consequence of the vanishing chemical potentials under the assumption of vanishing lepton and baryon asymmetry and, consequently, a vanishing neutral current tadpole contribution.

It is convenient to change integration variables, with

$$W \equiv W_p = \sqrt{q^2 + k^2 + M^2 - 2qk\cos(\varphi)} \Rightarrow \frac{dW}{d\cos(\varphi)} = -\frac{qk}{W_p}; \tag{4.20}$$

therefore,

$$\frac{d^3k}{W_p} = (2\pi)k^2 dk \frac{d(\cos(\varphi)}{W_p} = -(2\pi)\frac{kdkdW}{q}, \tag{4.21}$$

yielding

$$\mathrm{Im}[A(q_0,q) \mp B(q_0,q)] = \frac{g^2}{16\pi q}\int_{-\infty}^{\infty} dk_0 \int_0^\infty dk \int_{W_-}^{W+} dW L[Q^\pm;k] \cdot P[p]\bar{\rho}_f(k_0,k)\bar{\rho}_b(p_0,p)[1 - n_f(k_0) + N_b(p_0)], \tag{4.22}$$

where $p^0 = q^0 - k^0$. Now, in terms of the integration variables k^0, k, W,

$$\bar{\rho}_b = [\delta(q^0 - k^0 - W) - \delta(q^0 - k^0 + W)], \tag{4.23}$$

and the integration limits in W are

$$W^\pm = \sqrt{(q \pm k)^2 + M^2}. \tag{4.24}$$

The technical details of the calculation of the spectral densities are relegated to the Appendix, and we neglect the zero temperature contribution, assuming that it has been systematically absorbed by renormalization and focusing solely on the finite temperature terms.

A. Imaginary parts (damping rates)

We can now obtain the imaginary parts evaluated on the relativistic mass shells $q_0 \simeq q$ (for positive energy neutrinos). The analysis of the support for the delta functions in the Appendix shows that on the relativistic mass shell $q_0 = q$ the only contribution to the imaginary parts arises from the product (A13) with $k^+ = \infty$, $k^- = M^2/4q$,

$$-\delta(k^0 + k)\delta(q - k^0 - W_p); \qquad \vec{p} = \vec{q} + \vec{k},$$

corresponding to the process $W \to \bar{l}\nu_2$ [the anti lepton $\bar{l}$ is recognized in the delta function $\delta(k^0 + k)$ which determines that the energy is $-k$]. This is the contribution labelled 4 (A13) in the Appendix. The analysis of the regions of support in q_0 given by (A14)–(A16) shows a

remarkable phenomenon: the contributions (A14), (A16) describe the process of Landau damping [104], namely, the process of emission and reabsorption of thermal excitations in the medium that yields a branch cut below the light cone in the spectral density that vanishes at $T = 0$. These processes are the equivalent of those described in Ref. [104] for quarks interacting with gluons or electrons with photons. In these cases, namely, the exchange of massless vector bosons, the Landau damping cut ends at $q_0 = q$; however, for *massive* vector boson exchange, the Landau damping cut below the light cone *merges* with the branch cut above the light cone given by (A15). The mass shell for an ultrarelativistic sterilelike neutrino falls right at the end of the Landau damping cut and the beginning of the continuation above the light cone. It is precisely this point in the spectral density that contributes to the damping rate of the ultrarelativistic sterilelike neutrino and vanishes for $T = 0$. Therefore, the end point of the Landau damping cut yields the damping rate of the ultrarelativistic sterilelike neutrino, which, in turn, yields their *production rate* as a consequence of the detailed balance as discussed above.

This contribution to (4.8) yields

$$\begin{aligned}&\mathrm{Im}[A(q,q) \mp B(q,q)] \\ &= -\pi g^2 \int \frac{d^3k}{(2\pi)^3 4kW_p} L^{\mu\nu}[Q^{\pm};k] P_{\mu\nu}[p] \\ &\quad \times [n_f(k) + N_b(W_p)]\delta(W_p - q - k),\end{aligned} \tag{4.25}$$

which is *precisely* the expression for the rate Γ_2 in the quantum kinetic equation (3.14) with ultrarelativistic neutrinos and charged leptons[1] [up to the prefactor $\sin^2(\theta)$]. The helicity suppression factor arises similarly to the discussion after (3.16).

For negative helicity, the terms $F_1(q^0 = q, q) = 1$ and $F_2(q^0 = q, q) = 0$, and with the definitions (2.52), we find for negative $(-)$ and positive $(+)$ helicities respectively

$$\mathrm{Im}\Sigma^{-}(q) = \frac{g^2 T}{16\pi}\frac{M^2}{q^2}\ln\left[\frac{1 + e^{-M^2/4qT}}{1 - e^{-M^2/4qT}e^{-q/T}}\right] \tag{4.26}$$

$$\begin{aligned}\mathrm{Im}\Sigma^{+}(q) = \frac{g^2 T}{16\pi}\Bigg\{&\ln\left[\frac{1 + e^{-M^2/4qT}}{1 - e^{-M^2/4qT}e^{-q/T}}\right] \\ &+ \frac{2T}{q}\sum_{n=1}^{\infty}\frac{e^{-nM^2/4qT}}{n^2}\left(e^{-nq/T} - (-1)^n\right)\Bigg\}.\end{aligned} \tag{4.27}$$

These expressions clearly show the suppression for $q \ll M$ for $M \simeq T$ as a consequence of the fact that the decay products feature energy $\simeq M/2$. These results pertain generically to a vector boson of mass M, and we must add the contributions from the charged and neutral vector bosons with their respective masses and couplings. Anticipating the study with cosmological expansion in the next sections, we take as a reference mass that of the W vector boson M_w and introduce the dimensionless variables

$$\tau \equiv \frac{M_W}{T}; \qquad y = \frac{q}{T} \tag{4.28}$$

with the standard model relations (4.3).

Defining

$$\begin{aligned}&L[\tau,y] = \ln\left[\frac{1 + e^{-\tau^2/4y}}{1 - e^{-\tau^2/4y}e^{-y}}\right]; \\ &\sigma[\tau,y] = \frac{2}{y}\sum_{n=1}^{\infty}\frac{e^{-n\tau^2/4y}}{n^2}(e^{-ny} - (-1)^n); \\ &\quad c \equiv \cos(\theta_w) \simeq 0.88\end{aligned} \tag{4.29}$$

the sum of the contributions yield for $\gamma^{\mp}(q)$ (2.55), (2.56)

$$\gamma^{-}(\tau;y) = M_W\frac{\alpha_w\tau}{y^2}\left[\frac{1}{8}L[\tau,y] + \frac{1}{16c^4}L[\frac{\tau}{c},y]\right] \tag{4.30}$$

$$\begin{aligned}\gamma^{+}(\tau;y) = \alpha_w M_W\left(\frac{M_s}{M_W}\right)^2\frac{\tau}{4y^2}\Bigg\{&\frac{1}{8}(L[\tau,y] \\ &+ \sigma(\tau,y)) + \frac{1}{16c^2}\left(L\left[\frac{\tau}{c},y\right] + \sigma\left[\frac{\tau}{c},y\right]\right)\Bigg\}.\end{aligned} \tag{4.31}$$

The helicity suppression of the positive helicity rate $\gamma^{+}(q)$ is manifest in the ratio M_s^2/M_W^2; this is expected on the grounds that the typical momentum of the emitted neutrino is $\simeq M_W/2$. As a function of $y = q/T$, the rates feature a maximum at $\simeq\tau^2/8$, and they are displayed in Figs. 2 and 3.

The suppression of the imaginary parts on shell (damping rates) as $y \to 0$ has a simple explanation: for a vector boson of mass M decaying at rest in the plasma into two relativistic leptons, energy conservation implies that each lepton carries a momentum $M/2$, and for $\tau \simeq 1$, this implies $y \simeq 1/2$. For the neutrino to feature $y \ll 1$, it must be that the massive vector boson is *highly boosted* in the plasma, but the probability of such a state is exponentially suppressed, thus resulting in an exponential suppression of low momentum neutrinos.

For the mixing angles in the medium (2.44), we need $\gamma^{\pm}(q)/\xi$ with ξ given by (2.41), namely,

$$\begin{aligned}&\frac{\gamma^{-}(\tau;y)}{\xi} = \left(\frac{M_W}{M_s}\right)^2 I^{-}(\tau;y); \\ &I^{-}(\tau,y) = \frac{2\alpha_w}{y}\left[\frac{1}{8}L[\tau,y] + \frac{1}{16c^4}L\left[\frac{\tau}{c},y\right]\right]\end{aligned} \tag{4.32}$$

[1]The lepton tensor $L_{\mu\nu}$ is in terms of $Q^{\pm}$ that is divided by the energy of the relativistic neutrino [see the definitions (2.51)].

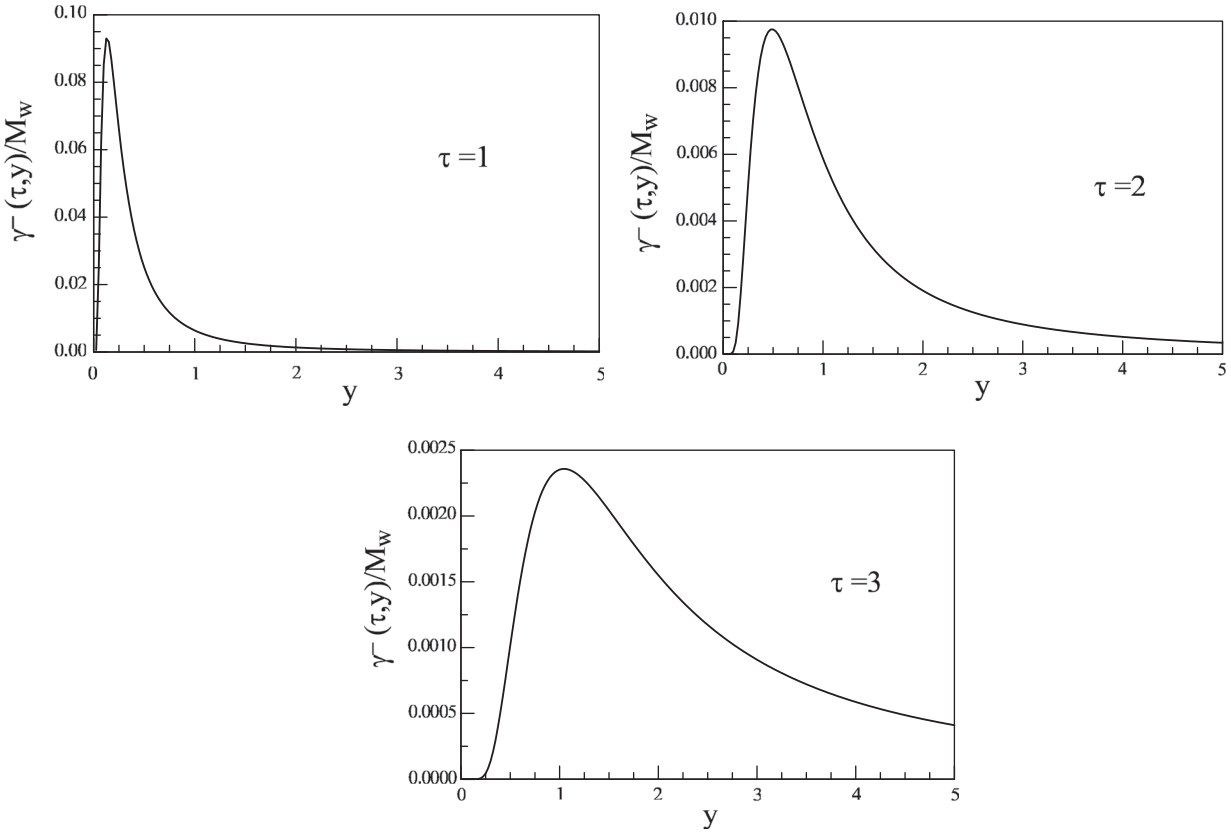

FIG. 2. $\gamma^{-}(q)/M_W$ given by Eq. (4.30) vs $y = q/T$ for $\tau = M_W/T = 1, 2, 3$ respectively.

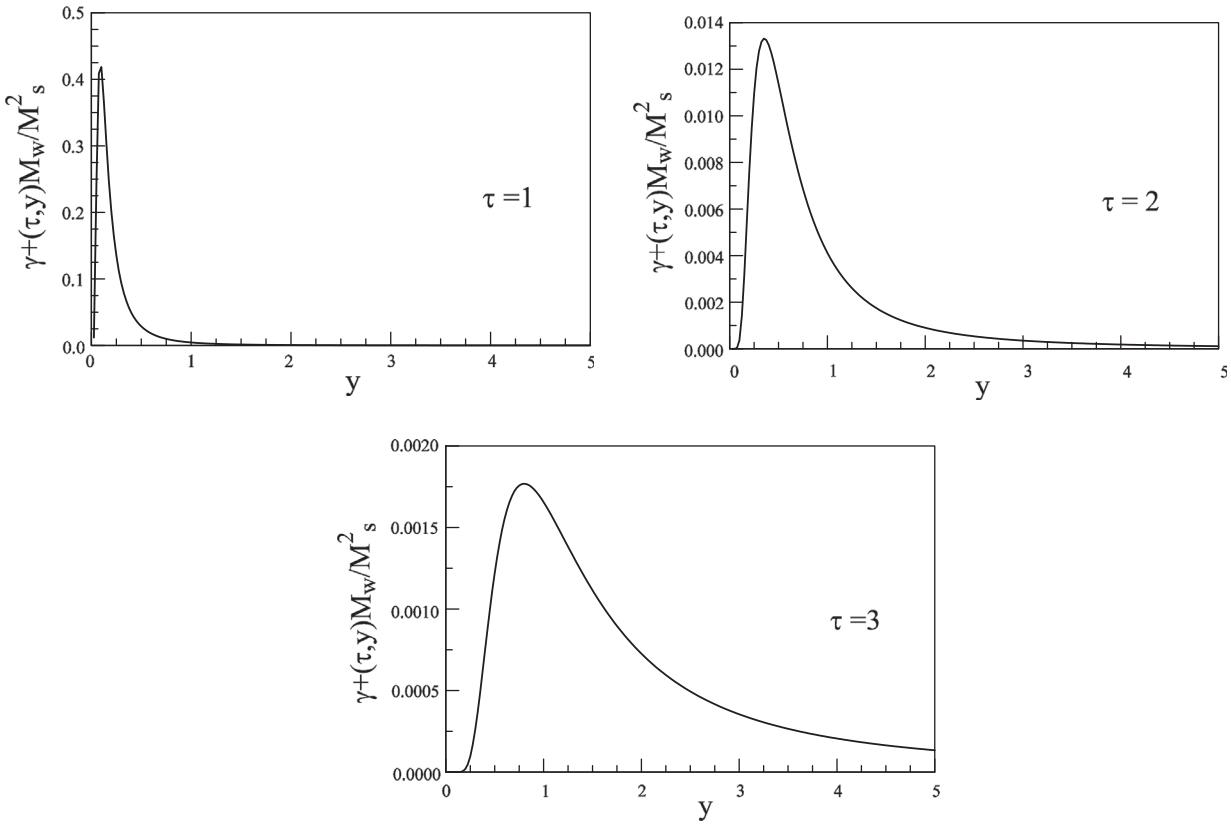

FIG. 3. $\gamma^{+}(q)M_W/M_s^2$ given by Eq. (4.31) vs $y = q/T$ for $\tau = M_W/T = 1, 2, 3$ respectively.

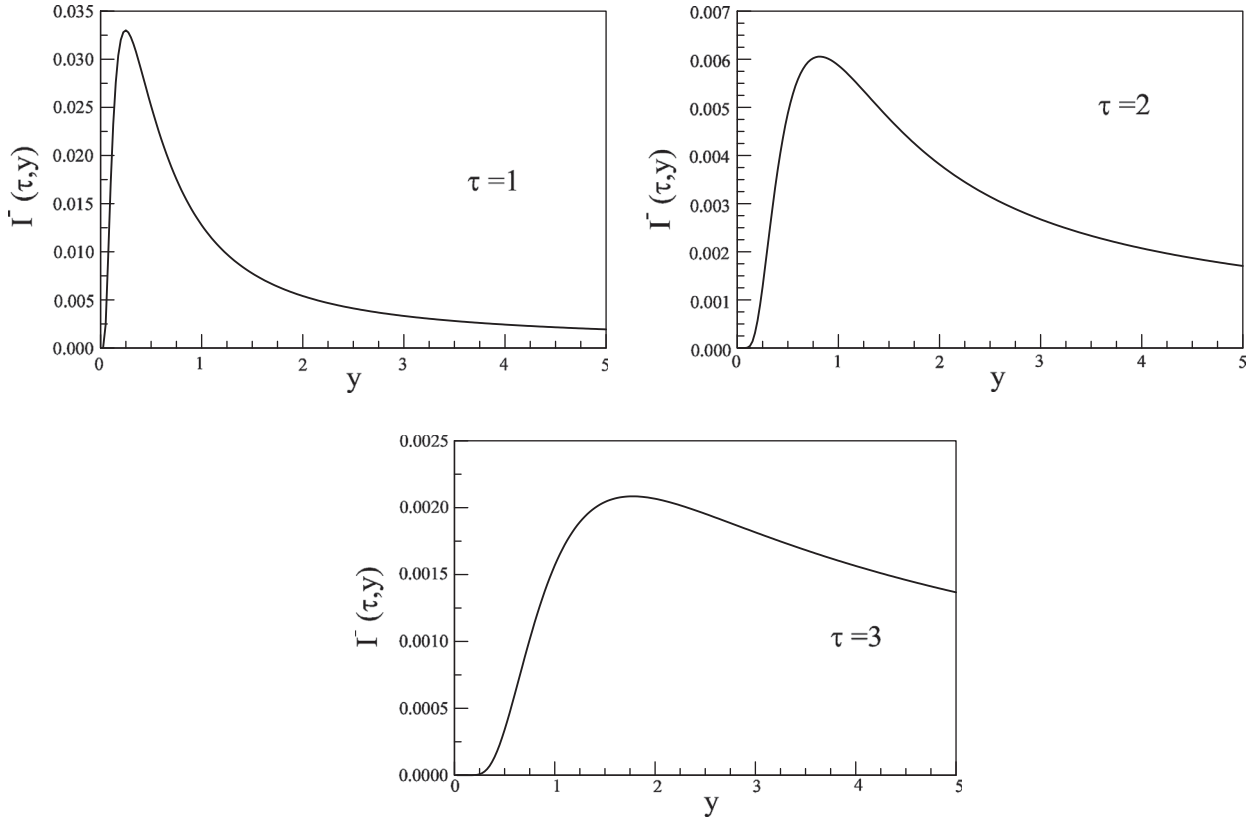

FIG. 4. $I^{-}(\tau, y)$ given by Eq. (4.32) vs $y = q/T$ for $\tau = M_W/T = 1, 2, 3$ respectively.

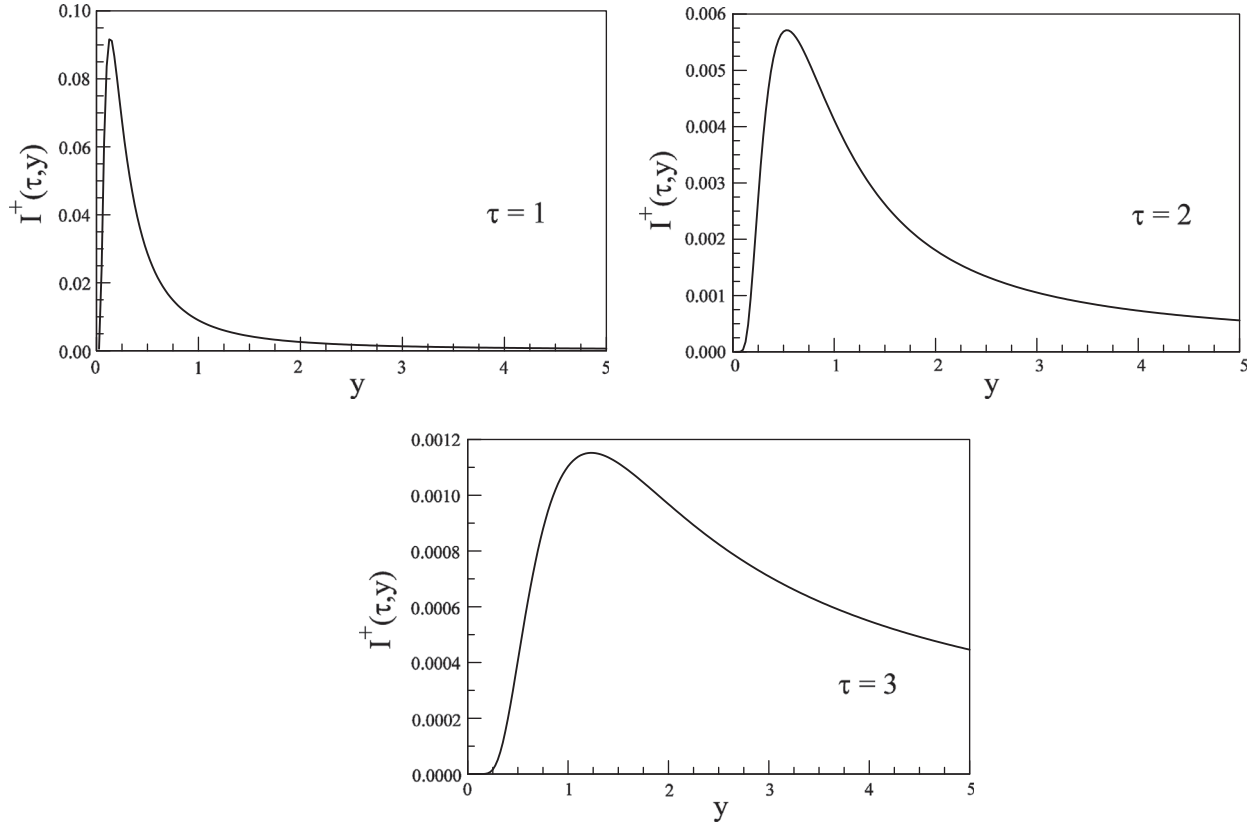

FIG. 5. $I^{+}(\tau, y)$ given by Eq. (4.33) vs $y = q/T$ for $\tau = M_W/T = 1, 2, 3$ respectively.

$$\frac{\gamma^+(\tau;y)}{\xi} \equiv I^+(\tau;y) = \frac{\alpha_w}{2y}\left\{\frac{1}{8}(L[\tau,y]+\sigma(\tau,y)) + \frac{1}{16c^2}\left(L\left[\frac{\tau}{c},y\right]+\sigma\left[\frac{\tau}{c},y\right]\right)\right\}. \tag{4.33}$$

Figures 4 and 5 display $I^{\mp}(\tau,y)$ for $\tau = 1, 2, 3$. The main observation is that $I^{\mp} \ll 1$ in the whole range of y for $\tau \gtrsim 1$. This is important. Note that γ^-/ξ is *enhanced* by the factor M_w^2/M_s^2; therefore, for $M_W/M_s \gtrsim 10^2$, it follows that $\gamma^-/\xi \gg 1$ for $\tau \gtrsim 1$ for $y \simeq 1$, and this will result in a large suppression of the effective mixing angle in the medium. On the other hand, the helicity suppression implies that $\gamma^+/\xi = I^+(\tau,y) \ll 1$ in the whole range of y for $\tau \geq 1$, and this will result in a vanishingly small correction to the effective mixing angle in the medium, which in this case will be nearly the same as that for the vacuum. These points will be revisited again below when we discuss the corrections to the mixing angle *vis-à-vis* the production rate in the expanding cosmology.

V. REAL PART: INDEX OF REFRACTION

The index of refraction or real part of the self-energy is obtained from the dispersive representation (2.14). In the Appendix, we provide the details of the calculation of $\mathrm{Re}\Sigma^{\mp}$; both are of the form

$$\mathrm{Re}\Sigma^{\mp}(q) = \frac{g^2 T}{16\pi^2}\frac{M^2}{q^2}\mathcal{K}^{\mp}\left[\frac{M}{T},\frac{q}{T}\right], \tag{5.1}$$

where $\mathcal{K}^{\mp}[\tau,y]$ are dimensionless functions of the ratios M/T; $y = q/T$, and are calculated numerically, implementing the steps detailed in the Appendix. Combining the contributions from charged and neutral currents, we find

$$\mathrm{Re}\Sigma^{\mp}(\tau,y) = M_W\frac{\tau}{y^2}\frac{\alpha_w}{4\pi}\left[\frac{1}{2}\mathcal{K}^{\mp}[\tau,y]+\frac{1}{4c^4}\mathcal{K}^{\mp}\left[\frac{\tau}{c},y\right]\right]. \tag{5.2}$$

Of relevance for the in-medium mixing angle are the ratios $\Delta^{\pm}/\xi$ with $\Delta^{\pm}$ given by (2.57) and (2.58) and ξ given by (2.41).

A. Negative helicity

For negative helicity, with the definitions (2.41), (2.57), we find

$$\frac{\Delta^-(q)}{\xi} = \left(\frac{M_W}{M_s}\right)^2 J^-(\tau,y), \tag{5.3}$$

where

$$J^-(\tau,y) = \frac{\alpha_w}{2\pi y}\left[\frac{1}{2}\mathcal{K}^-[\tau,y]+\frac{1}{4c^4}\mathcal{K}^-\left[\frac{\tau}{c},y\right]\right]. \tag{5.4}$$

B. Low temperature limit

The limit $\tau \gg 1; \tau \gg y$ $(q \ll M_w)$ affords an analytic treatment, the details of which are summarized in the Appendix. In this limit, we find that the general form of the real part of the self-energy is given by

$$\mathrm{Re}\Sigma^-(q) = \frac{14\pi^2}{90}g^2\left(\frac{T}{M}\right)^4 q; \tag{5.5}$$

adding the charged and neutral current contributions, we find in this limit

$$\mathrm{Re}\Sigma^-_{\mathrm{tot}}(\tau,y) = M_W\frac{28\pi^3\alpha_w}{90}\left[1+\frac{1}{2}\cos^2(\theta_w)\right]\frac{y}{\tau^5}, \tag{5.6}$$

which agrees with those of Refs. [92,103], and

$$\frac{\Delta^-}{\xi} = \frac{28\pi^3\alpha_w}{45}\left(\frac{M_W}{M_s}\right)^2\left[1+\frac{1}{2}\cos^2(\theta_w)\right]\frac{y^2}{\tau^6}. \tag{5.7}$$

C. Positive helicity

For positive helicity, with the definitions (2.41), (2.58), we find

$$\frac{\Delta^+(q)}{\xi} = J^+(\tau,y), \tag{5.8}$$

where

$$J^+(\tau,y) = \frac{\alpha_w\tau^2}{8\pi y^3}\left[\frac{1}{2}\mathcal{K}^+[\tau,y]+\frac{1}{4c^4}\mathcal{K}^+\left[\frac{\tau}{c},y\right]\right]. \tag{5.9}$$

Figure 7 displays $J^+(\tau,y)$ vs y for $\tau = 1, 2$; we see that $J^+ \ll 1$ for all values of y diminishing rapidly as a function of τ. This results in a small (and negligible) correction to the mixing angle in the medium.

D. Low temperature limit

As in the previous case, the limit $\tau \gg 1; \tau \gg y$ $(q \ll M_w)$ can be obtained analytically; see the Appendix for details. The general form of the real part of the self-energy in this case is

$$\mathrm{Re}\Sigma^+(q) = \frac{14\pi^2}{180}g^2\left(\frac{T}{M}\right)^4 q; \tag{5.10}$$

adding the charged and neutral current contributions, we find in this limit

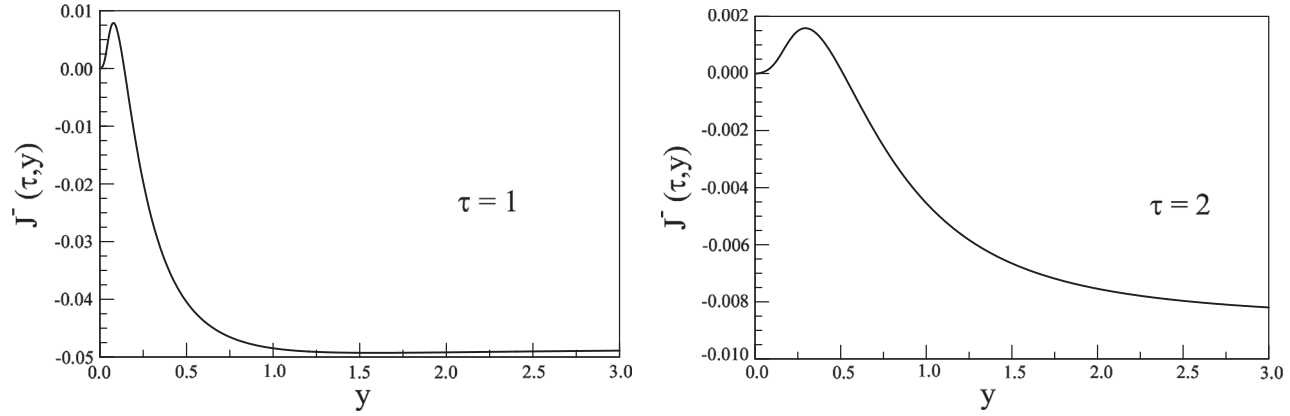

FIG. 6. $J^-(\tau, y)$ Eq. (5.4) vs $y = q/T$ for $\tau = M_W/T = 1, 2$ respectively.

$$\mathrm{Re}\Sigma^+_{\mathrm{tot}}(\tau, y) = M_W \frac{28\pi^3\alpha_w}{180}\left[1 + \frac{1}{2}\cos^2(\theta_w)\right]\frac{y}{\tau^5}; \qquad (5.11)$$

and adding the charged and neutral current contributions and including the helicity suppression factor, we find

$$\frac{\Delta^+}{\xi} = \frac{7\pi^3\alpha_w}{90}\left[1 + \frac{1}{2}\cos^2(\theta_w)\right]\frac{1}{\tau^4}. \qquad (5.12)$$

VI. EFFECTIVE MIXING ANGLES AND PRODUCTION RATES

The effective mixing angles are given by (2.62), and in the previous sections, we obtained $\Delta^\pm/\xi$ and $\gamma^\pm/\xi$.

A. Negative helicity

For negative helicity, Δ^-/ξ is given by (5.3), and γ^-/ξ is given by (4.32); therefore,

$$\theta^2_{\mathrm{eff}}(\tau, y) = \frac{\theta^2(\frac{M_s}{M_W})^4}{[(\frac{M_s^2}{M_W^2} + J^-(\tau, y))^2 + (I^-(\tau, y))^2]}. \qquad (6.1)$$

Figures 4 and 6 display $I^-(\tau, y), J^-(\tau, y)$ as a function of y for various values of τ. These show important features: J^- vanishes and becomes negative at a value of $y^*(\tau)$ that increases monotonically with τ. This behavior implies that for $M_W \gg M_s$ the vanishing of $J^-(\tau, y)$ implies a MSW resonance in the absence of lepton asymmetry for the effective mixing angle for *negative helicity*. However, this resonance is "screened" by the contribution to the mixing angle from the imaginary part, inspection of both J^- and I^- (see Figs. 4 and 6) and an exhaustive numerical study reveal that in the broader region $0 < y^*(\tau) \lesssim y$ the imaginary part I^- yields the dominant contribution to the denominator of (6.1) and there is no substantial enhancement of the mixing angle as y sweeps through the resonance for any τ. In other words, the presence of the MSW resonance does not influence the effective mixing angle in a substantial manner. The numerical analysis shows that for $M_s/M_W \lesssim 10^{-2}$ the term $(M_s/M_W)^2$ in the denominator in (6.3) can be safely neglected and the effective mixing angle is $\propto (M_s/M_W)^4$, reflecting a strong in-medium suppression, even when the denominator becomes large because J^-, I^- are very small as shown in the figures. The smallness of the denominator is thus compensated by the large power of $M_s/M_W \ll 1$ in the numerator.

In the low temperature limit $T \ll M_W$, the effective mixing angle in the medium is given by

$$\theta_{\mathrm{eff}}(\tau, y) = \frac{\theta}{[1 + \frac{28\pi^3\alpha_w}{45}(\frac{M_W}{M_s})^2[1 + \frac{1}{2}\cos^2(\theta_w)]\frac{y^2}{\tau^6}]}, \qquad (6.2)$$

and the contribution from the imaginary part is subleading as it is suppressed by an extra power of α_w from two loop contributions to the self-energy.

The production rate [see Eqs. (2.59) and (3.19)] is

$$\Gamma^-_{\mathrm{prod}}(\tau, y) = \frac{M_W\theta^2(\frac{M_s}{M_W})^4}{y[e^y + 1]}\frac{\tau I^-(\tau, y)}{[(\frac{M_s^2}{M_W^2} + J^-(\tau, y))^2 + (I^-(\tau, y))^2]}. \qquad (6.3)$$

Although both J^- and I^- vanish as $y \to 0$, and the effective mixing angle reaches its maximum ($\theta_{\mathrm{eff}} \to \theta$), the imaginary part I^- vanishes exponentially as $y \to 0$, and the production rate vanishes in this limit. The effect of the MSW resonance is screened by the imaginary part, and the resulting production rate features a peak as a function of y for fixed τ that is a result of the competition between the peak in $I^-(y, \tau)$ (see Fig. 4) and the increase in $(J^-)^2$.

We will analyze further the production rate in the following section within the context of cosmological expansion.

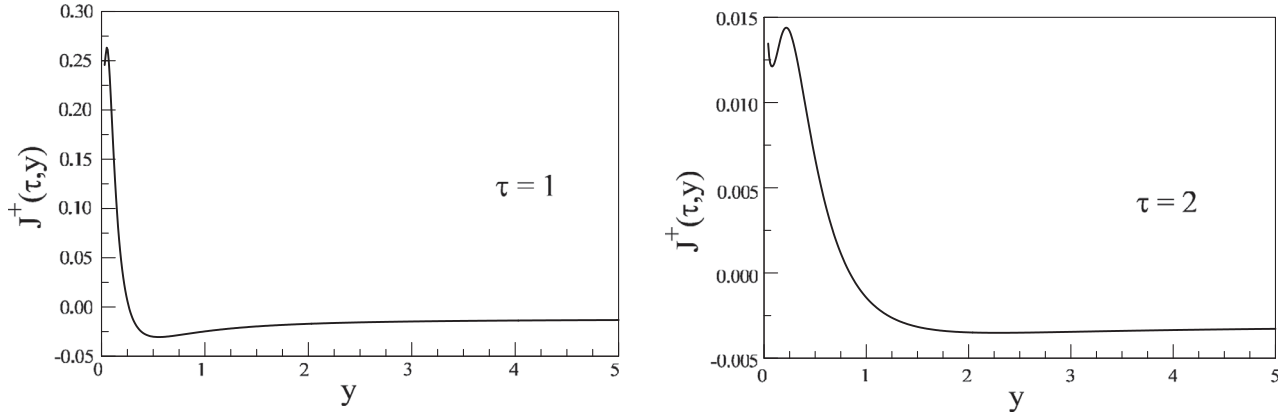

FIG. 7. $J^+(\tau, y)$ Eq. (5.9) vs $y = q/T$ for $\tau = M_W/T = 1$, 2 respectively.

B. Positive helicity

For positive helicity, the effective mixing angle is given by

$$\theta^2_{\rm eff}(\tau, y) = \frac{\theta^2}{[(1 + J^+(\tau, y))^2 + (I^+(\tau, y))^2]}, \tag{6.4}$$

and the production rate

$$\Gamma^+_{\rm prod}(\tau, y) = \frac{M_W \theta^2 (\frac{M_s}{M_W})^2}{y[e^y + 1]} \frac{\tau I^+(\tau, y)}{[(1 + J^+(\tau, y))^2 + (I^+(\tau, y))^2]}. \tag{6.5}$$

From Figs. 5 and 7, we see that I^+, $J^+ \ll 1$ in the region in which I^+ peaks, and therefore we can set $J^+ \simeq 0; I^+ \simeq 0$ in the denominator in (6.5). In other words, the in-medium contribution to the mixing angle is negligible; namely, $\theta_{\rm eff} \simeq \theta$, and we can approximate the production rate of positive helicity neutrinos as

$$\Gamma^+_{\rm prod}(\tau, y) \simeq M_W \theta^2 \left(\frac{M_s}{M_W}\right)^2 \frac{\tau I^+(\tau, y)}{y[e^y + 1]}. \tag{6.6}$$

This is an important result. The helicity suppression entails a *much weaker coupling to the medium*, which in turn results in a negligible in-medium correction to the mixing angles and the effective mixing angle is the same as the vacuum mixing angle.

The positive helicity production rate is $\propto (M_s/M_W)^2$ as a consequence of helicity suppression, whereas the negative helicity production rate (6.3) is $\propto (M_s/M_W)^4$ as a consequence of the in-medium suppression of the mixing angle but is enhanced by the small denominator. As will be discussed below, there is a range of masses and temperatures for which the negative and positive helicity rates are *comparable*: positive helicity states feature helicity suppressed couplings but nearly vacuum mixing angles, whereas negative helicity states feature stronger coupling to the medium, which in turn leads to strongly suppressed in-medium mixing angles. This aspect is studied below.

VII. COSMOLOGICAL PRODUCTION

We consider a spatially flat Friedmann-Robertson-Walker cosmology during a radiation dominated stage. The effect of cosmological expansion is included by replacing the momentum in Minkowski space-time with the physical momentum in the expanding cosmology, namely,

$$q \to \frac{q}{a(t)}, \tag{7.1}$$

where $a(t)$ is the scale factor and now q refers to the (constant) comoving momentum. As we focus on the production during the radiation dominated era, the physical temperature is

$$T(t) = \frac{T_0}{a(t)}, \tag{7.2}$$

where T_0 is the temperature that the plasma would have *today* as we normalize the scale factor to 1 today. We note that the variable

$$y = \frac{q(t)}{T(t)} = \frac{q}{T_0} \tag{7.3}$$

is a *constant* under cosmological expansion in terms of the comoving momentum and the temperature that the plasma would feature today.

In terms of the comoving wave vector q and the invariant ratio $y = q/T$, the quantum kinetic equation in the expanding cosmology reads

$$\frac{dn^h_2(q;t)}{dt} = \Gamma^h_2(q, t)[n_{eq}(q) - n^h_2(q;t)], \tag{7.4}$$

where now $\Gamma_2^h(q,t) \equiv \Gamma_2^h(\tau(t),y)$ depends on time through $\tau(t) = M_W/T(t) = M_W a(t)/T_0$,

Under the assumption of $\theta \ll 1$ and a vanishing initial population, we neglect the buildup of the population and approximate the quantum kinetic equation as

$$\frac{dn_2^h(t)}{dt} = \Gamma^h_{\rm prod}(\tau(t),y), \tag{7.5}$$

where $\Gamma^{\mp}_{\rm prod}(\tau(t),y)$ are given by (6.3) and (6.5). Since the production rate depends on time through $\tau(t)$, it is convenient to use this variable in the kinetic equation, with

$$\frac{dn_2^h(t)}{dt} = \frac{dn_2^h(\tau,y)}{d\tau} H(t)\tau(t), \tag{7.6}$$

where during radiation domination

$$H(t) = \frac{\dot{a}(t)}{a(t)} = 1.66 g_{\rm eff}^{1/2}(T)\frac{T^2(t)}{M_{pl}};$$
$$M_{pl} = 1.22 \times 10^{19}\ \text{GeV}. \tag{7.7}$$

$g_{\rm eff}(T)$ is the effective number of relativistic degrees of freedom, $g_{\rm eff} \simeq 100$, and varies slowly in the temperature regime $1\ \text{GeV} < T < 100\ \text{GeV}$. We will approximate $g_{\rm eff} \simeq 100$ and constant in this temperature range, anticipating that freeze-out will occur at $T_f \simeq$ few GeV.

A. Negative helicity

For negative helicity, we find

$$\frac{dn_2^-(\tau,y)}{d\tau} \simeq \frac{0.92\times 10^{16}\theta^2(\frac{M_s}{M_W})^4}{y[e^y+1]} \times \frac{\tau^2 I^-(\tau,y)}{[(\frac{M_s^2}{M_W^2} + J^-(\tau,y))^2 + (I^-(\tau,y))^2]}. \tag{7.8}$$

As both J^- and I^- decrease as the temperature decreases (and τ increases), there are two competing effects: the damping rate $\propto I^-$ decreases, but the effective mixing angle increases as a result; for a fixed value of $y = q/T$, the production rate peaks as a function of τ and falls off sharply. We write (7.8) as

$$\frac{dn_2^-(\tau,y)}{d\tau} \equiv 0.92\times 10^{16}\theta^2\left(\frac{M_s}{M_W}\right)^4 R^-(y,\tau). \tag{7.9}$$

As discussed above, for $M_s/M_W < 10^{-2}$, we find numerically that $R^-(y,\tau)$ is nearly independent of M_s. The form (7.9) separates the suppression factor from the effective mixing angle in terms of the prefactor $\theta^2 M_s^4/M_w^4$, whereas for $M_s/M_W < 10^{-2}$, the function $R^-(y,\tau)$ is *insensitive to the value of* M_s and only depends on standard model couplings and vector boson masses. As τ increases (temperature decreases), the effective mixing angle increases, whereas the damping rate γ^- *decreases*; therefore, we expect $R^-(y,\tau)$ for fixed values of y to feature a peak as a function of τ. The analysis in the previous sections clarifies that for $\tau \gg \sqrt{y}$ the damping rate is exponentially suppressed [see Eqs. (4.30) and (4.29)], whereas the real part (index of refraction) falls off as $1/\tau^5$ [see Eq. (5.7)]; therefore, the production rate is exponentially suppressed at large τ as the mixing angle grows much slower. This entails the *freeze-out* of the distribution function.

This expectation is confirmed by the numerical study. Figures 8 and 9 show $R^-(y,\tau)$ for various values of y as a function of τ and as a function of y for $\tau = 2,\ 5,\ 10$. Numerically, the case with $M_s/M_W = 10^{-4}$ is indistinguishable from that setting $M_s = 0$ in the denominator of R^- [see Eq. (7.8)]. These figures clearly show the "freeze-out" of the distribution as a function of τ; as the rate vanishes for large τ, larger values of y freeze out at larger τ but with much smaller amplitudes. This feature is expected; the vector bosons are suppressed at smaller temperatures (larger τ), and large values of y are further suppressed by the detailed balance factor $1/(e^y+1)$. Figure (9) shows the "filling" of the different wave vectors; as time evolves, larger y are populated, but eventually larger values of y are suppressed by the Fermi-Dirac factor $n_{eq}(y)$. *Assuming* that the initial population vanishes at $\tau \simeq 1$), the asymptotic distribution function is given by

$$n_2^-(y) = \int_1^\infty \frac{dn_2^-(\tau,y)}{d\tau} d\tau = 0.92\times 10^{16}\theta^2\left(\frac{M_s}{M_W}\right)^4 F^-(y), \tag{7.10}$$

where we have defined the *frozen* distribution

$$F^-(y) = \int_1^\infty R^-(y,\tau)d\tau, \tag{7.11}$$

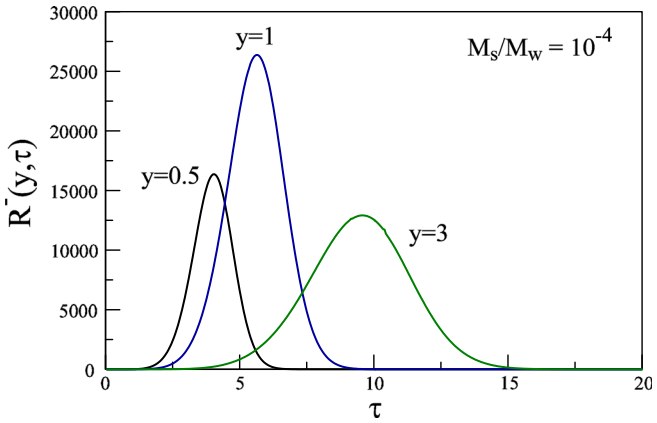

FIG. 8. Rates $R^-(y,\tau)$ [see Eqs. (7.8) and (7.9)] vs τ for $y = 0.5,\ 1,\ 3$ for $M_s/M_W = 10^{-4}$.

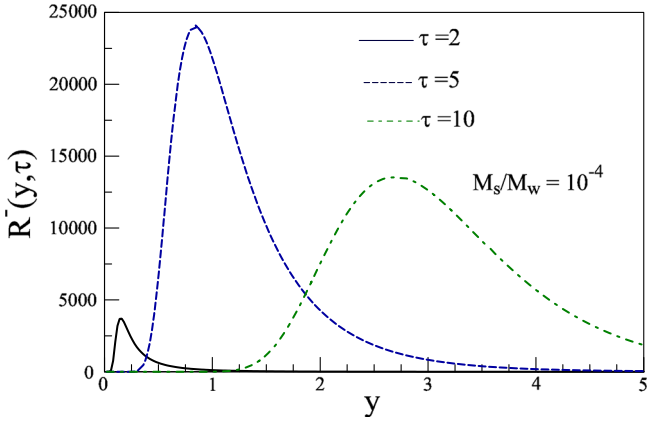

FIG. 9. Rates $R^{-}(y,\tau)$ vs y for $\tau = 2$, 5, 10 for $M_s/M_W = 10^{-}4$.

which is shown in Fig. 10. Although we have set the lower limit $\tau = 1$ for consistency in (7.11), we find that $R^{-}(y,\tau)$ vanishes as $\tau \to 0$ and the lower limit can be effectively taken to $\tau = 0$. A numerical study informs us that the region $0 < y \lesssim 10$, which features the largest contribution to the distribution function, freezes out at $\tau_f \simeq 15$, corresponding to a freeze-out temperature for negative helicity modes $T_f^{-} = M_W/\tau_f \simeq 5$ GeV.

The vanishing of $F^{-}(y)$ as $y \to 0$ is a consequence of the vanishing of the imaginary part and a direct consequence of the decay kinematics in the medium; as explained above, the $y \to 0$ is dominated by the decay of vector bosons that are highly boosted in the rest frame of the plasma, and the population of these states is highly suppressed at $T \simeq M_W$. The broadening of the distribution as compared to the damping rate (compare Figs. 4 and 10) is a consequence of a longer freeze-out time resulting from the competition between a decreasing damping rate I^{-} and an increasing mixing angle; the modes with higher y continue to populate as the mixing angle increases, but eventually as modes with large values of y are populated, their contribution is suppressed by the detailed balance factor $n_{eq}(y)$. After freeze-out, the total number density of negative helicity neutrinos produced (equal to the total number of positive helicity antineutrinos in the absence of a lepton asymmetry) is given by

$$\mathcal{N}_2^{-} = \frac{T^3(t)}{2\pi^2}\int_0^\infty n_2^{-}(y)y^2dy, \tag{7.12}$$

for which we need the result

$$\int_0^\infty y^2F^{-}(y)dy \equiv N^{-} = 2.287\times 10^6. \tag{7.13}$$

This integral is dominated by the region $0 < y \lesssim 10$, which freezes out at $\tau \simeq 15$, with the result that

$$\frac{\int_{10}^\infty y^2F^{-}(y)dy}{\int_0^\infty y^2F^{-}(y)dy} = 3.9\times 10^{-3}. \tag{7.14}$$

Normalizing the number density to that of 1 degree of freedom of an active massless neutrino decoupled in equilibrium at the *same* temperature, namely,

$$\mathcal{N}_\nu = \frac{T^3(t)}{2\pi^2}\int_0^\infty n_{eq}(y)y^2dy, \tag{7.15}$$

where $n_{eq}(y) = 1/(e^y+1)$, we find

$$\frac{\mathcal{N}_2^{-}}{\mathcal{N}_\nu} = 285\theta^2\left(\frac{M_s}{\text{MeV}}\right)^4; \tag{7.16}$$

this ratio is constant throughout the expansion history. This analysis shows that this mechanism of production will not yield a thermalized species for $M_s$few MeV and $\theta \ll 10^{-4}$, under these conditions, we note that the approximation (7.5) of neglecting the buildup of the population in the quantum kinetic equation (7.4) is consistent since the ratio $\mathcal{N}_2^{-}/\mathcal{N}_\nu \ll 1$.

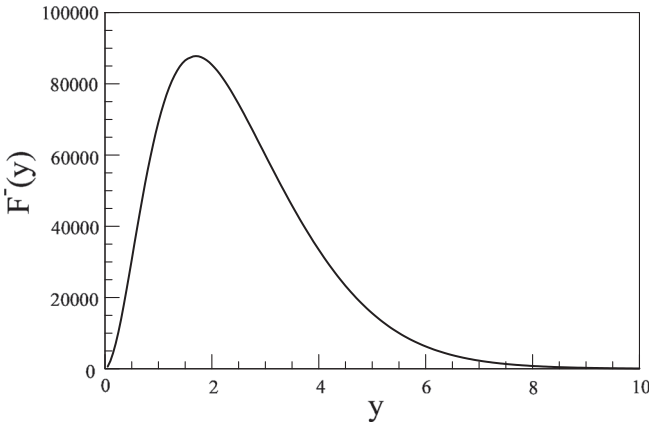

FIG. 10. Asymptotic distribution function $F^{-}(y)$ [see Eqs. (7.10) and (7.11)] vs y.

B. Positive helicity

For positive helicity, we find

$$\frac{dn_2^{+}(\tau,y)}{d\tau} \simeq 0.92\times 10^{16}\theta^2\left(\frac{M_s}{M_W}\right)^2\frac{\tau^2I^{+}(\tau,y)}{y[e^y+1]}, \tag{7.17}$$

where, as discussed above, we have used the approximate rate (6.6). As for the negative helicity case, it proves convenient to write (7.17) as

$$\frac{dn_2^{+}(\tau,y)}{d\tau} \simeq 0.92\times 10^{16}\theta^2\left(\frac{M_s}{M_W}\right)^2R^{+}(y,\tau);$$
$$R^{+}(y,\tau) = \frac{\tau^2I^{+}(\tau,y)}{y[e^y+1]}, \tag{7.18}$$

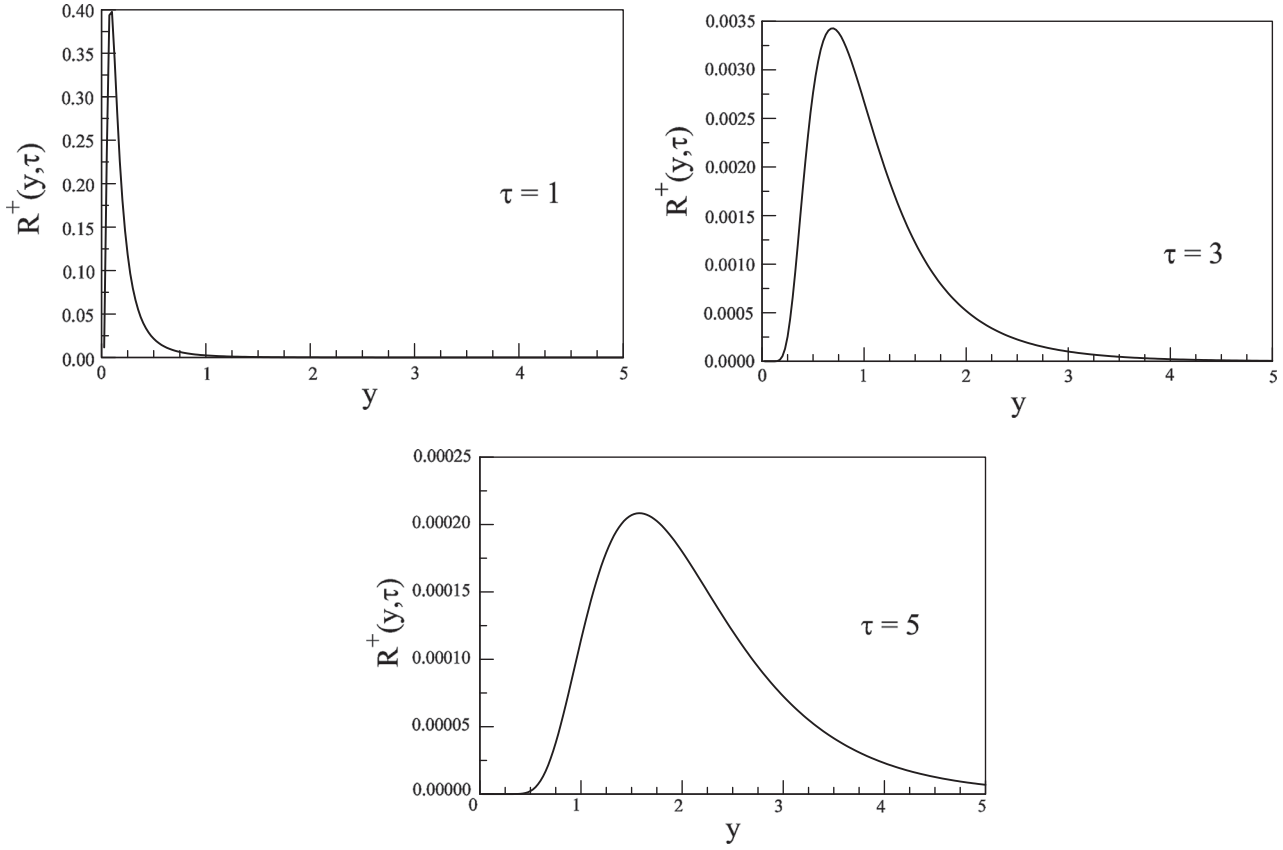

FIG. 11. $R^+(\tau, y)$ given by Eq. (7.18) vs $y = q/T$ for $\tau = 1, 3, 5$ respectively.

where $R^+(\tau, y)$ is read off (7.17) and does not depend on M_s. Figure 11 shows $R^+(\tau, y)$ vs y for $\tau = 1, 3, 5$, and Fig. 12 shows $R^+(\tau, y)$ vs τ for $y = 1, 3, 5$. Together, these figures show the filling of higher momentum modes as the temperature decreases and the freeze-out of the distribution function for different wave vectors. The larger values of y take longer to be populated and freeze out later, but their contribution is strongly suppressed by the detailed balance factor $1/(e^y + 1)$.

Similarly to the previous case, the asymptotic distribution function is

$$n_2^+(y) = 0.92 \times 10^{16}\theta^2\left(\frac{M_s}{M_W}\right)^2 F^+(y);$$
$$F^+(y) = \int_1^\infty R^+(\tau, y)d\tau. \tag{7.19}$$

The asymptotic distribution function $F_2^+(y)$ is shown in Fig. 13; it is dominated by the region $0 < y \lesssim 8$ with

$$\frac{\int_8^\infty y^2F^+(y)dy}{\int_0^\infty y^2F^+(y)dy} = 3.3 \times 10^{-3} \tag{7.20}$$

and freezes out at $\tau \simeq 10$, corresponding to a freeze-out temperature $T_f^+ \simeq 8$ GeV.

We note that the distribution function for the positive helicity component is sharply peaked at small momenta $y \approx 0.5$ as compared to that for the negative helicity component, which is much broader and peaks at $y \simeq 2.5$; namely, the positive helicity component yields a much *colder* distribution (compare Figs. 10 and 13). The reason for this discrepancy is the fact that the production rate for the negative helicity component features a competition between a diminishing damping rate but an increasing effective mixing angle as τ increases (temperature decreases). This competition results in a longer freeze-out time allowing buildup in the population of larger momentum modes as τ evolves as discussed above. It is remarkable that the distribution functions $F_2^\pm$ are very similar to those found from pion decay in Refs. [45,89]. The similarity is more striking for F^-. The physical reason for this similarity is actually simply the fact that low momentum modes are suppressed since the presence of low momentum sterile neutrinos in the decay of a much more massive particle implies that this "mother" particle must be highly boosted in the plasma.

The total population at an asymptotically long time is given by

$$\mathcal{N}_2^+ = \frac{1}{2\pi^2}\int_0^\infty n_2^+(y)y^2dy, \tag{7.21}$$

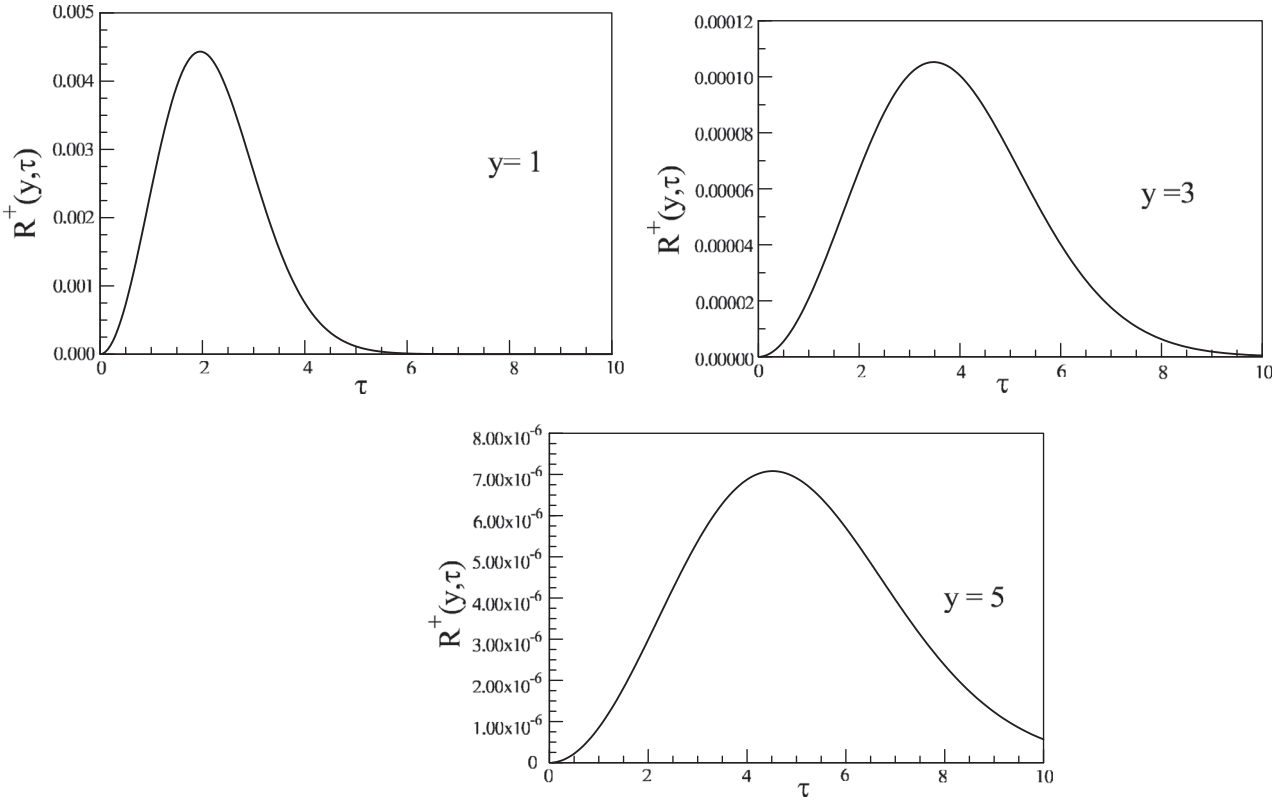

FIG. 12. $R^+(y,\tau)$ vs τ for $y = 1, 3, 5$.

which is determined by the integral

$$\int_0^\infty y^2 F^+(y)dy \equiv N^+ = 0.025. \tag{7.22}$$

As in the negative helicity case, normalizing to the number density of relativistic neutrino decoupled in equilibrium at the same temperature (7.15), we find

$$\frac{\mathcal{N}_2^+}{\mathcal{N}_\nu} \simeq 2 \times 10^4 \theta^2 \left(\frac{M_s}{\text{MeV}}\right)^2. \tag{7.23}$$

Again, we see that for $M_s \simeq$ MeV and $\theta \ll 10^{-2}$ the sterilelike species produced by vector boson decay *does not thermalize*.

We have studied the contributions of positive and negative helicity individually to highlight the different distribution functions and dependence on M_s; however, each is simply a different decay channel for the production of sterilelike eigenstates from the decay of vector bosons, and both channels contribute to the total abundance. Hence, we combine both channels to give the total density

$$\begin{aligned} n_2(y) &= n_2^+(y) + n_2^-(y) \\ &= 3.6\left(\frac{\theta^2}{10^{-4}}\right)\left(\frac{M_s}{\text{MeV}}\right)^2 f(M_s, y); \\ f(M_s, y) &= \left[\frac{F^+(y)}{N^+} + \left(\frac{M_s}{8.35\ \text{MeV}}\right)^2 \frac{F^-(y)}{N^-}\right], \end{aligned} \tag{7.24}$$

where the normalization factors $N^\pm$ are given by (7.13) and (7.22). The effective distribution function multiplied by the phase space factor y^2 is shown in Fig. 14 for $M_s = 1$ MeV where is dominated by the *positive helicity component* and $M_s = 10$ MeV where it is dominated by the *negative helicity component*.

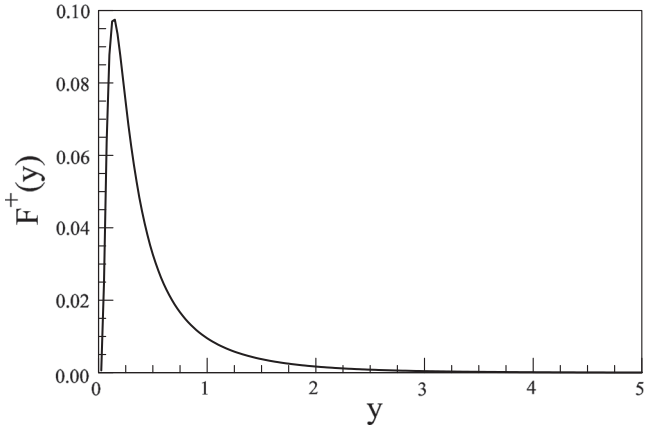

FIG. 13. Asymptotic distribution function $F^+(y)$ in Eq. (7.19) vs $y = q/T$.

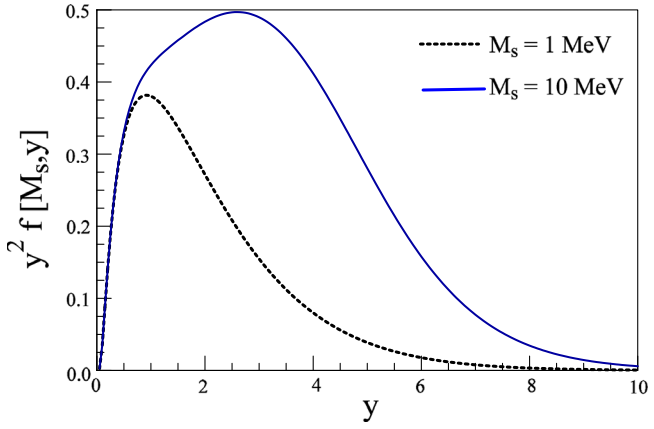

FIG. 14. Total distribution function $f(M_s, y)$ in Eq. (7.24) multiplied by y^2 vs $y = q/T$ for $M_s = 1; 10$ MeV.

This figure clearly shows the strongly nonthermal total distribution function at freeze-out. It also provides a specific example of the "mixed dark matter" nature [89] when several different production channels with different kinematics and effective mixing angles contribute to the production of a sterilelike species. The "hump" in $f(M_s, y)$ for $M_s = 10$ MeV is a result of the competition between the two channels; the negative helicity channel is hotter since its distribution is peaked at larger momenta but becomes dominant at larger M_s, whereas that of the positive helicity is colder since it is peaked at lower momenta but dominates for smaller M_s. Accordingly, we find for the total abundance normalized to that of a single degree of freedom of a massless thermal neutrino, with $\mathcal{N}_2 = \mathcal{N}_2^+ + \mathcal{N}_2^-$,

$$\frac{\mathcal{N}_2}{\mathcal{N}_\nu} \simeq 2\left(\frac{\theta^2}{10^{-4}}\right)\left(\frac{M_s}{\text{MeV}}\right)^2\left[1+\left(\frac{M_s}{8.35\ \text{MeV}}\right)^2\right]. \quad (7.25)$$

The first term in the brackets is the contribution from the positive helicity states, and the second is from the negative helicity; both become comparable for $M_s \simeq 8.35$ MeV.

If the sterilelike neutrino is *stable*, its comoving number density would remain constant, and upon becoming nonrelativistic, this species would contribute to dark matter a fraction given by [89]

$$\mathcal{F}_2 = \frac{\Omega_{\nu_2}h^2}{\Omega_{\text{DM}}h^2} = \frac{M_s}{7.4\ \text{eV}}\left(\frac{g_{\nu_2}}{g_d}\right)\int_0^\infty n_2(y)y^2dy, \quad (7.26)$$

where g_{ν_2} is the number of degrees of freedom for neutrinos of negative helicity; we will assume Dirac neutrinos in which case $g_{\nu_2} = 2$, accounting for neutrinos and antineutrinos ($g_{\nu_2} = 1$ for Majorana neutrinos); and $g_d \simeq 100$ is the number of ultrarelativistic degrees of freedom at decoupling (freeze-out), which occurs at $T_f \simeq 5-8$ GeV, yielding

$$\mathcal{F}_2 = 0.97\left(\frac{\theta^2}{10^{-8}}\right)\left(\frac{M_s}{\text{MeV}}\right)^3\left[1+\left(\frac{M_s}{8.35\ \text{MeV}}\right)^2\right]. \quad (7.27)$$

The terms in the brackets are the contribution from the positive helicity and negative helicity, respectively, and the latter dominates for $M_s \gg 8.35$ MeV.

It is clear from this expression that the sterile neutrinos produced by vector boson decay *cannot* yield a substantial $\simeq$KeV warm dark matter component, since the x-ray data constrain such a component to the mass range $\simeq$few KeV and mixing angle $\theta^2 \lesssim 10^{-10}$ [33–35,43], which according to (7.27) would yield a negligible abundance of such species. However, accelerator and cosmological bounds [73,81] allow for heavy sterile states with masses in the MeV range and mixing angles $\lesssim 10^{-5}$; in fact, these are the bounds used in the recent analysis of MeV sterile neutrinos as possible solutions to the ^{7}Li problem [74,79], which we discuss further in Sec. VIII below.

The results obtained above for the distribution and abundances constitute a lower bound. This is because we have neglected any initial population, and, as it will be discussed below, we expect other processes to yield sterilelike neutrinos at various stages of the thermal history.

VIII. DISCUSSION

A. Validity of approximations

We have implemented several approximations to obtain the above results, which merit a discussion of their validity:

(i) Ultrarelativistic neutrinos: This is an obvious approximation for the activelike mass eigenstates; for the sterilelike eigenstate, this implies $M_s/q \ll 1$. In the expanding cosmology, this inequality is in terms of the physical momentum $q_{\text{phys}}(t) = q/a(t)$ with q being the comoving momentum. Since $y = q_{\text{phys}}(t)/T(t)$ is a constant and $T(t) = M_W/\tau$, hence $q_{\text{phys}}(t) = yM_W/\tau$. The inequality must be evaluated at freeze-out; therefore, the condition for the validity of the ultrarelativistic limit for sterilelike neutrinos is

$$\frac{yM_W}{M_s\tau_f} \gg 1, \quad (8.1)$$

in the range of the distribution function with the largest support. With $\tau_f \simeq 15$, the condition (8.1) applies to $y \gtrsim M_s/6$ GeV, which is fulfilled for $y \gtrsim 10^{-3}$ for $M_s \simeq$ few MeV. The distribution function is exponentially suppressed at small y in both cases; therefore, $M_s \simeq$ few MeV fulfills the criterion in almost the whole range but for extremely small values of y which are suppressed both by the distribution and by the phase space.

(ii) $\theta \ll 1$: This approximation was used in expanding the square roots in (2.28) and extracting the dispersion relations (2.39), (2.42), (2.43) and effective mixing angles (2.44). Assuming $\theta \ll 1$, the actual approximation is $(1+(\Delta/\xi))^2+(\gamma/\xi)^2 \gg \theta^2$ or in fact that $\theta_{\rm eff} \leq \theta$, which is fulfilled in both cases. As was discussed above in the negative helicity case, the (MSW) resonance when $1+\Delta_2/\xi \simeq 0$ is actually screened by the term $\gamma_2/\xi = (M_W^2/M_s^2)I^-$, which is actually $\gg 1$ for $M_W/M_s > 10^2$ suppressing the effective mixing angle $\theta_{\rm eff} \ll \theta$. Therefore, this approximation is consistent; namely, assuming that the vacuum mixing angle is $\ll 1$ implies that the effective mixing angle is also $\ll 1$ and the corrections are such that $\theta/\theta_{\rm eff} \leq 1$.

(iii) Activelike neutrinos in LTE: This approximation was invoked to obtain the neutral current contribution to the self-energy with thermalized neutrinos in the intermediate state. For $\theta \ll 1 \to \theta_{\rm eff} \ll 1$ and $\cos(\theta_{\rm eff}) \simeq 1$ implying that the interaction vertices of activelike neutrinos are the usual standard model ones. This, in turn, implies the validity of the usual argument that leads one to conclude that active neutrinos are in LTE down to $T \simeq$ MeV, which is much smaller than the freeze-out temperature of sterilelike neutrinos $T_f \simeq$ few GeV. Therefore, this approximation is valid all throughout the region of production via vector boson decay and even much lower temperatures down to the usual decoupling temperature $\simeq$MeV for weak interactions.

(iv) Perturbative expansion: The validity of perturbation theory in describing sterilelike production and freeze-out relies on *two* small dimensionless parameters: $\alpha_w \simeq 1/32$ and $\theta \ll 1$. Inspection of the ratio $\delta\omega_2^h/\omega_2(q)$ [see Eqs. (2.39) and (2.42)] clearly shows that this ratio is $\ll 1$ for $\theta_{\rm eff} \ll 1$, $\alpha_w \ll 1$ and the ultrarelativistic limit, confirming the validity of the perturbative expansion for the description of production and freeze-out of sterilelike neutrinos.

B. Other contributions and higher orders

Production of sterilelike neutrinos from vector boson decay is the *dominant* process at $T \simeq M_{W,Z}$ and is of order α_w as clearly exhibited by the results obtained above. This is the leading contribution to the self-energy in this temperature range, namely, the one-loop contributions depicted in Fig. 1. In the same temperature regime, there are several other processes that contribute to the imaginary part of the self-energy and hence to the production rate: heavy quark and lepton decays via charged current interactions, $q \to q\bar{\nu}\nu$, $\tau, \mu \to \bar{\nu}\nu l$; charged lepton annihilation $l^+l^- \to \bar{\nu}\nu$ (via neutral currents); and several other processes (for a more detailed discussion, see Ref. [89]). These processes contribute to the imaginary part of the self-energy at *two loops* and therefore are of order α_w^2. Furthermore, at $T \ll M_{W,Z}$, these are further suppressed by a vector boson propagator, and therefore their contribution to the imaginary part is generically $CG_F^2T^4q$ typically with $C \simeq 1$. As the temperature diminishes through the cosmological expansion, the damping rate from vector boson decay will become of the same order as the contribution to the imaginary part from these higher order processes, which must then be taken into account if the available energy is larger than the threshold for sterilelike production. Therefore, the results obtained in the previous section provide a lower bound to the abundance of sterilelike neutrinos, as processes that are of higher order but dominate at lower temperatures increase the abundance.

The index of refraction, namely, the real part of the self-energy, is dominated by the one-loop result, which for low temperatures (large τ) is given by the low temperature limits (5.6), (5.11). This observation is important. At $T \ll M_W$ on dimensional grounds, the two loop processes yield real and imaginary parts of the self-energy $\propto G_F^2T^4q$ since this limit is well described by the local Fermi theory; therefore, compared to the low temperature limit of the *one-loop* contribution (5.6), (5.11), the two-loop contribution to the real part is suppressed by a power of α_w. Therefore, for $T \ll M_W$, the leading contribution to real part or index of refraction is given by the one-loop results (5.6), (5.11), whereas the imaginary part (damping rate) is determined by the two-loop diagrams and are $\propto G_F^2T^4q$, the proportionality constant determined by the nature and number of degrees of freedom (leptons and quarks) that enter in the processes. Therefore, in principle, a complete description of production and freeze-out should include all possible processes at one and two loops in the self-energy. The real part is dominated by the one-loop term, but the imaginary part will receive contributions from both one and two loops; the relevance of each will depend on the temperature regime. For the mixing angle, both the real and imaginary part (damping rate) are needed, however the imaginary part is of the same order than the real part only for the one-loop contribution, namely at temperatures of the order of $M_{W,Z}$ (or larger), however, at much lower temperatures, the corrections to the mixing angle are dominated by one-loop contribution to the real part given by (5.7), (5.12) and the two loop contributions to both the real and imaginary parts can be safely neglected in agreement with the results of Refs. [13,20,103]. Reference [26] discusses further contributions at $T \gg M_W$ which merit further study but are outside the scope of this article.

In the temperature regime considered here, $T \simeq M_{W,Z}$, self-energy corrections to the propagators of massive vector bosons (quark and lepton loops) are perturbative and suppressed by another power of α_w. Self-energy corrections to the charged lepton propagators are the same as the hard thermal loop corrections. In Sec. IV, we discussed the possible influence of hard thermal loop corrections to the

lepton propagators, arguing that these are subleading for kinematic reasons. The numerical results obtained in the previous sections confirm this argument; the production rate and final distribution functions receive the largest support in the region of momenta $q/T \lesssim 2-3$. In this region of phase space, kinematically the charged leptons produced via vector boson decay feature momenta $q \simeq T$, and in this region of momenta, hard thermal loop corrections can be safely neglected. However, the large momentum tail of the sterile neutrino distribution, although strongly suppressed as shown numerically, will be affected by these corrections. A study of these is beyond the scope of this article and is relegated to a future study.

C. Lifetime constraints

Massive sterilelike neutrinos can decay in various leptonic channels [58,59]. Consider the simpler case of one sterilelike ν_2 and one activelike ν_1 neutrino with $\theta \ll 1$, the charged current channel $\nu_2 \to e^+e^-\nu_1$ is available for $M_2 \simeq M_s > 1$ MeV. The "invisible" neutral current $\nu_2 \to 3\nu_1$ channel is available for any M_s of cosmological relevance for WDM or cold dark matter. The radiative channel $\nu_2 \to \gamma\nu_1$ is suppressed by one power of α_{em}. The decay widths for these channels have been obtained [58,59,105] as

$$\Gamma(\nu_2 \to e^+e^-\nu_1) \simeq 3.5 \times 10^{-5}\theta^2 \left(\frac{M_s}{\mathrm{MeV}}\right)^5 K\left[\frac{m_e^2}{M_s^2}\right]\left(\frac{1}{s}\right), \tag{8.2}$$

where the function $K \to 0$ for $M_s \to 2m_e$ and $K \to 1$ for $M_s \gg m_e$ [58]. For other leptonic channels, similar expressions were obtained in Ref. [105].

The decay rate into activelike neutrinos mediated by neutral currents [not Glashow-Iliopoulos-Maiani suppressed with sterilelike heavy neutrinos] is given by (see Refs. [58,59])

$$\Gamma(\nu_2 \to 3\nu_1) \simeq 3.5 \times 10^{-5}\theta^2 \left(\frac{M_s}{\mathrm{MeV}}\right)^5 \left(\frac{1}{s}\right) \tag{8.3}$$

and the radiative decay width [59,106]

$$\Gamma(\nu_2 \to \gamma\nu_1) \simeq 10^{-7}\theta^2 \left(\frac{M_s}{\mathrm{MeV}}\right)^5 \left(\frac{1}{s}\right). \tag{8.4}$$

Recent results for a lower bound on the lifetime of dark matter yields $t_b \simeq 160$ Gyr [107]; a similar bound but in terms of the fraction of cold dark matter is given in Ref. [108]. Adding both leptonic channels, assuming that $M_s \gtrsim$ MeV and taking both of the same order, the condition that the sterile species would be a suitable dark matter candidate implies that its lifetime is longer than or equal to this lower bound, namely, $\Gamma_{\mathrm{tot}} t_b \leq 1$, implying that

$$\theta^2 \left(\frac{M_s}{\mathrm{MeV}}\right)^5 \lesssim 10^{-14}. \tag{8.5}$$

Combining this bound with the fractional abundance (7.27), we find that

$$\frac{\mathcal{F}_2 \left(\frac{M_s}{\mathrm{MeV}}\right)^2}{\left[1 + \left(\frac{M_s}{8.35\ \mathrm{MeV}}\right)^2\right]} \lesssim 10^{-6}, \tag{8.6}$$

which could yield $\mathcal{F}_2 \simeq 1$ for $M_s \simeq$ few KeV, which, however, would require a very large mixing angle $\theta \simeq 10^{-2}$ which is ruled out by cosmological x-ray bounds [33–35,43]. Hence, we conclude that sterilelike neutrinos produced via vector boson decay cannot be suitable dark matter candidates.

However, if there is a hierarchy of sterilelike neutrinos, heavy neutrinos with M_s of a few MeV and mixing angles $\theta^2 \gg 10^{-13}$, these may decay into lighter ≃KeV sterilelike states that could contribute to the dark matter abundance. This possibility of cascade decay merits further study and is clearly beyond the scope of this article.

D. Comparison to other results

The expressions for the quantum kinetic equation (3.17) and the effective mixing angle in the medium (2.44) that we obtained are exact to all orders in standard model couplings and to leading order in $\theta^2 \ll 1$. In Refs. [27,109], an expression for the effective mixing angle that includes both the real part (index of refraction) and imaginary part (damping rate) of the self-energy (from standard model interactions) has been proposed that seems to be valid for an arbitrary vacuum mixing angle. Our result is only valid for $\theta \ll 1$ where we can extract unambiguously the mixing angle from the position of the complex poles in the propagator. It is not straightforward to define or extract a real mixing angle in the case of large θ; the subtleties are discussed in Ref. [92]. The final form of the quantum kinetic equation (3.17) is similar to that used in Refs. [11,13], although in these articles, the mixing angle only includes the index of refraction (real part), valid in the temperature regime of interest in those articles. Crucially, our analysis shows the importance of the positive helicity component: at high temperature, the in-medium suppression of the mixing angle for negative helicity is much larger than that for positive helicity since the latter interacts with the medium with a coupling that is helicity suppressed. However, the contributions from the in-medium suppressed negative helicity and the helicity suppressed positive helicity may be competitive within a range of masses and temperatures. This is an aspect that has not been discussed previously.

Reference [26] considers the production of ≃GeV sterile neutrinos in the temperature range $5\ \mathrm{GeV} < T < 160\ \mathrm{GeV}$, focusing on the washout of lepton densities;

our results are in broad agreement with those of this reference for the processes associated with vector boson decay for negative helicity states in the regions where a comparison is meaningful. However, in contrast, we focus on the mass scale $\simeq$MeV motivated by the possible solution to the ^{7}Li problem and concentrate on the role which helicity plays in the effective mixing angles in the medium and the damping and production rates. Furthermore, we study the full dynamics of production and freeze-out, including cosmological expansion for both helicity states obtaining the abundance at freeze-out and establishing the freeze-out temperature and time scales for each helicity.

The role that helicity plays is an immediate consequence of the $V-A$ coupling in the standard model. The interaction of positive helicity states with the medium is helicity suppressed, relative to those with negative helicity. As shown above, the mixing angle for positive helicity states is hardly modified by their interaction with the medium, whereas that for negative helicity states is strongly suppressed, positive helicity states dominate the production in a wide range of masses. Furthermore, we find a MSW resonance for negative helicity states in the absence of a lepton asymmetry, which is screened by the damping rate and does not enhance the production. We study the full dynamics of production with cosmological expansion analyzing the freeze-out of both helicity states, establishing the freeze-out temperature for each channel and obtaining the frozen distributions. The final distribution exhibits the contribution from both helicity channels, one colder than the other and with both distinctly nonthermal. We also analyze the various accelerator, lifetime and cosmological constraints both for dark matter as well as the possibility that $\simeq$MeV sterile neutrinos might solve the ^{7}Li problem (see the discussion below).

E. Thermalization?

The result for the total abundance of sterile neutrinos produced via vector boson decay, compared to that of a thermal species given by Eq. (7.25), shows that for $\theta \ll 10^{-2}$, and M_s of few MeV sterile neutrinos produced via this mechanism do not thermalize. If the lifetime of the sterilelike neutrino is (much) shorter than the age of the Universe, it means that at some time in the past history of the Universe the rate $dn_s(t)/dt < 0$ since if such a species is present today its population is decaying in time. We have argued that the quantum kinetic equation (3.17) is exact to all orders in standard model couplings to leading order in $\theta^2 \ll 1$. In fact, as per the discussion leading up to (3.17), the production term is completely determined by the damping rate, the mixing angle (in the combination Γ_2^h) and detailed balance, which, if the sterilelike mass eigenstate is not relativistic, entails that the correct form of the quantum kinetic equation is

$$\frac{dn_2^h(q;t)}{dt} = \Gamma_2^h(q)[n_{\rm LTE}(E) - n_2^h(q;t)], \tag{8.7}$$

where

$$n_{\rm LTE}(E) = \frac{1}{e^{\frac{E}{T}}+1}; \qquad \frac{E}{T} = \sqrt{y^2 + \frac{M_2^2}{T^2}} \tag{8.8}$$

and $\Gamma_2^h(q)$ are the damping rates in terms of the imaginary part of the self-energy (2.59). In Minkowski space-time, however small, the mixing angle (hence Γ_2) sterilelike mass eigenstates will *always* thermalize; the longer the thermalization time scale, the smaller Γ_2. With cosmological expansion, freeze-out occurs when $\Gamma_2/H(t) \ll 1$ (for a more detailed discussion, see Ref. [89]). In the original form (gain-loss) of the kinetic equation (3.4), the gain term always involves the annihilation of one or several species (vector bosons, leptons and quarks) that by assumption are in LTE in the plasma; as the Universe expands and cools, the abundance of these species diminishes, and the gain contributions diminish accordingly. The loss terms that involve the annihilation of one or more species in LTE also diminish under cosmological expansion; however, if the sterile neutrino can decay into other species, this decay contribution only entails the *creation* of the decay products, and these contributions do not vanish as the temperature diminishes. Three processes that contribute to the loss term and survive in the low temperature limit are precisely the decay channels (8.2), (8.3), (8.4). Therefore, if the sterilelike mass eigenstate decays with a lifetime smaller than the age of the Universe, these loss terms dominate the quantum kinetic equation at some late time, and the rate becomes negative before today. The form (8.7) implies that at some time in the past the sterilelike neutrino has *thermalized*, since the production term (gain) dominates initially but the decay (loss) dominates at late times, the rate must have passed through zero in between, namely the distribution reached LTE and started to decay after this point. This discussion becomes relevant with the possibility that M_s of a few MeV and lifetime $\simeq 10^5(s)$ could provide a solution to the ^{7}Li problem as suggested in Refs. [74,78,79], as discussed below.

In Ref. [110], a study of low scale type-I seesaw models suggests that processes that are dominant at much lower temperature result in the thermalization of heavy states. Therefore, it is possible that other mechanisms which dominate at lower temperature and are not considered in our study may lead to the thermalization of the heavy sterile states produced via vector boson decay. An important aspect to be understood is whether thermalization occurs before or after the time scale required to solve the ^{7}Li problem [79] as this will impact the destruction of ^{7}Be in the nucleosynthesis chain.

The study of such a possibility is definitely important but beyond the scope of this article.

F. Solution to the ^{7}Li problem?

In Ref. [79], the authors performed an exhaustive analysis of the parameter space within which the decay of sterile neutrinos of $M_s \simeq$ few MeV could yield a solution to the ^{7}Li problem as previously advocated in Refs. [74,78]. The analysis of Ref. [79] included the most recent data on cosmic microwave background anisotropies and concluded that a heavy sterile neutrino with $M_s \simeq 4.35$ MeV and lifetime $\Gamma^{-1} \simeq 1.8 \times 10^5(s)$ would provide a suitable solution. However, the parameter space also bounds the ratio[2] $\mathcal{N}_s/\mathcal{N}_\nu \simeq 10^{-4}$ and the mixing angle $\theta^2 \simeq 10^{-4}$. These values are in significant tension both with the results that we obtained above and the bounds of Ref. [83]. In particular, with $M_s \simeq$ few MeV and such a large mixing angle, our result (7.25) indicates that $\mathcal{N}_s/\mathcal{N}_\nu \simeq 1$, suggesting full thermalization; furthermore, as is discussed above, our results provide a lower bound for the abundance of sterilelike heavy neutrinos. Both the region of abundance and mixing angles found in Ref. [79] seem in strong tension with the bounds in Ref. [83], and both caveats are recognized in Ref. [79], which suggests, as a possible alternative, a low reheating temperature [73]. Of course, our results rely on LTE at the electroweak scale; therefore, they are not applicable to such a scenario. Hence, although the production mechanism of sterilelike neutrinos studied in this article, which is the leading order in standard model couplings and provides a lower bound to the abundance, offers a compelling mechanism for production of heavy sterilelike neutrinos with the possibility to solve the ^{7}Li problem, significant tension arises between the parameter range of the solution established in Ref. [79], our result as a lower bound on the abundance and the cosmological bounds obtained in Ref. [83]. The resolution of this tension merits a deeper study, well beyond the scope of this article.

G. WDM from cascade decay

The analysis of the solution to the ^{7}Li problem suggested in Refs. [74,78,79] is a specific example of a cascade decay mechanism: heavy ($M_s \sim$ few MeV) sterilelike neutrinos produced at a (high) scale that eventually decay into several channels with the daughter particles influencing important physical processes during cosmological expansion. If there is a hierarchy of sterilelike massive neutrinos that include MeV and KeV scales, the heavier mass states may be produced at a high temperature, such as explored in this article, and the decay of this heavy state on a time scale $\simeq 10^5 s$ to solve the ^{7}Li problem (if the caveats discussed above can be overcome) can also lead to the production of the lighter mass states that can be suitable WDM candidates. While this lifetime is interesting within the context of the ^{7}Li problem, a heavy neutrino with $M_s \simeq$ MeV and $\theta \simeq 10^{-7}$ would feature a lifetime $\simeq 10^{12}(s)$ therefore decaying into a WDM candidate just after matter radiation equality. This possibility emerges naturally by writing the weak interaction vertices in mass eigenstates, and then the process $\nu_2 \to 3\nu_1$ yields a contribution $\nu_2 \to 2\nu_1\nu_m$ with ν_2 and ν_m the heavier ($\simeq$MeV) and lighter ($\simeq$KeV) mass eigenstates, respectively. The branching ratio for such a process is $\propto \theta_m^2$, where θ_m^2 is the mixing angle of the active (flavor) neutrinos with the sterilelike lighter neutrino ν_m. This mechanism of production of WDM candidates is a tantalizing possibility that would be a natural scenario in extensions beyond the standard model that posit the existence of several sterile neutrinos merits further study clearly beyond the scope of this article.

IX. SUMMARY OF RESULTS, CONCLUSIONS AND FURTHER QUESTIONS

Our goals in this article are twofold:

(i) First is to obtain the general form of the quantum kinetic equations and effective mixing angles in the medium to describe production and freeze-out of sterilelike (mass eigenstates) neutrinos in a broad range of temperatures and under a minimal set of assumptions. Our study departs from previous ones (see the recent review [111]) in several important aspects: we focus on the different helicity contributions, and we systematically include the absorptive part of the self-energy in the in-medium modification of the mixing angle.

(ii) Second is to apply the kinetic equations thus found to study the production to leading order in standard model couplings from vector boson decay at $T \simeq M_W$.

We obtained the effective mixing angles in the medium directly from the equations of motion in the case of mixing of one sterile with one active neutrino via a seesaw mass matrix with standard model interactions for the active (flavor) neutrino valid when the vacuum mixing angle $\theta \ll 1$ but to all orders in standard model couplings. Assuming that all standard model degrees of freedom are in LTE in the relevant temperature range, we obtained the quantum kinetic equation that describes the production, evolution and freeze-out of sterilelike mass eigenstates. The mixing angles in the medium and the production rate are determined by the real and imaginary parts of the self-energy on the mass shell of the sterilelike mass eigenstate and depend on helicity. The full quantum kinetic equation to leading order in $\theta \ll 1$ is

$$\frac{dn_2^h(q;t)}{dt} = \Gamma_2^h(q)[n_{\rm LTE}(q) - n_2^h(q;t)],$$

where $h = \pm$ correspond to helicity states and $\Gamma_2^{\mp}(q)$ are given by (2.59) with (2.55) and (2.55) and $n_{\rm LTE}$ is the

[2]This reference actually bounds $\mathcal{N}_s/\mathcal{N}_{cmb}$, which differs by a factor 3/4.

Fermi-Dirac distribution function in LTE. The full expression for the mixing angles in the medium, valid to all orders in standard model couplings and to leading order in $\theta \ll 1$, is given in the relativistic limit by

$$\theta^h_{\rm eff}(q) = \frac{\theta}{[(1+\frac{\Delta^h(q)}{\xi})^2 + (\frac{\gamma^h(q)}{\xi})^2]^{1/2}},$$

where Δ, γ, ξ are given by (2.55)–(2.58), (2.41), respectively, in terms of the real (Δ) and imaginary (γ) parts of the active neutrino self-energy on the mass shell of the sterilelike eigenstate.

We implemented the quantum kinetic equation to obtain the production of sterilelike neutrinos from vector boson decay at $T \simeq M_W$ including cosmological expansion. For negative helicity neutrinos (and positive helicity antineutrinos), the effective mixing angle is strongly suppressed by the medium; however, for positive helicity neutrinos (and negative helicity antineutrinos), the medium corrections are negligible because the interaction with the medium is helicity suppressed. We find that there is a region of masses for which the production of both species is comparable.

It is noteworthy that the mixing angle for negative helicity neutrinos features an MSW resonance in the absence of lepton asymmetry, which, however, is screened by the imaginary part of the self-energy. This is an important aspect that has not been previously addressed before; the absorptive (imaginary) part of the self-energy *also* contributes to the mixing angle in the medium.

Negative helicity neutrinos freeze out at $T^-_f \simeq 5$ GeV with a broader distribution as a consequence of a competition between a diminishing damping rate γ and an increasing effective mixing angle as the temperature diminishes. Positive helicity neutrinos' freeze-out temperature is $T^+_f \simeq 8$ GeV with a distribution that peaks at much smaller momenta, describing a colder species. Accounting for both channels, we find that the distribution function of sterilelike neutrinos of mass $M_2 \simeq M_s$ is given by

$$n_2(y) = 3.6\left(\frac{\theta^2}{10^{-4}}\right)\left(\frac{M_s}{\rm MeV}\right)^2 f(M_s, y),$$

where $y = q/T$ and $y^2 f(M_s, y)$ is strongly nonthermal and is displayed in Fig. 14, revealing the competition between the colder (positive helicity) and hotter (negative helicity) components. The total abundance normalized to that of one relativistic degree of freedom in thermal equilibrium ($\mathcal{N}_\nu$) is

$$\frac{\mathcal{N}_2}{\mathcal{N}_\nu} \simeq 2\left(\frac{\theta^2}{10^{-4}}\right)\left(\frac{M_s}{\rm MeV}\right)^2\left[1+\left(\frac{M_s}{8.35\ {\rm MeV}}\right)^2\right]. \qquad (9.1)$$

The first term in the brackets is the contribution from the positive helicity states, and the second is from the negative helicity; both become comparable for $M_s \simeq 8.35$ MeV. We argue that this expression is a lower bound on the abundance of sterilelike neutrinos.

The fractional abundance of dark matter contributed by both helicity components is given by (7.27). Constraints from x-ray data on masses and mixing angles suggest that sterilelike neutrinos produced by vector boson decay cannot yield a substantial $M_s \simeq$ KeV warm dark matter component. However, this production mechanism yields a substantial abundance of $M_s \simeq$ MeV heavy sterilelike neutrinos with $\theta^2 < 10^{-4}$ consistent with accelerator constraints. Therefore, this production mechanism may yield the heavy neutrinos recently invoked to solve the ^{7}Li problem [74,78,79]. However, the parameter range determined in Ref. [79] also bounds $\mathcal{N}/\mathcal{N}_\nu \simeq 10^{-4}$, which is incompatible with the result (9.1) for the range of mass and mixing angles reported in this reference and is also in conflict with recent bounds reported in Ref. [83]. The possibility that heavy ≃MeV sterilelike neutrinos decaying after BBN injecting energy in the medium providing a solution of the ^{7}Li problem as suggested also in Refs. [74,78,79] merits a deeper study both of the production mechanism as well as the cosmological impact of this heavy neutrino species.

A. Further questions

The study of production at $T \gg M_{W,Z}$ requires a deeper understanding of the finite temperature corrections to the dispersion relations of the vector bosons near the electroweak crossover regime, a worthy study which is beyond the scope of this article. We have suggested several other processes that contribute to the production throughout the thermal history of the Universe; while these are higher order (two loops) processes, they may be comparable to the leading order processes or even dominate at temperature $T \ll M_W$. However, the medium corrections to the mixing angles are completely determined by the one-loop contribution, and the effective mixing angle is given by Eq. (6.2). Further study of these processes is clearly warranted; they can be competitive near the freeze-out temperature of the leading one-loop contribution for heavy sterile neutrinos and, crucially, contribute to the production of lighter mass eigenstates. We have also argued that sterile neutrinos with lifetimes shorter than the age of the Universe that are decaying today must necessarily have thermalized at some time in the past. Studying this thermalization process is of fundamental interest since most of the calculations of production neglect this possibility by neglecting the loss term in the kinetic equation, yet thermalization of heavy sterile neutrinos may have important cosmological consequences for the expansion history. In Ref. [110], a study of low scale type-I seesaw models suggests that heavy sterile neutrinos do thermalize through collision processes dominant at much lower temperatures, motivating further studies of thermalization. We have also suggested that

several compelling extensions beyond the standard model posit a hierarchy of sterile neutrino masses, and this opens the possibility that heavier sterile states may be produced at high temperature, as analyzed here, and decay well after BBN or near the time of matter-radiation equality into lighter sterile states that may be suitable WDM candidates. This mechanism of cascade decay, which is fundamentally similar to that advocated for the solution to the ^{7}Li problem as an energy injection mechanism, is worthy of study.

ACKNOWLEDGMENTS

The authors thank Mikko Laine and Goran Senjanovic for bringing their work to the authors' attention. D. B. and L. L. gratefully acknowledge support from the NSF through Grant No. PHY-1506912. L. L. and R. D. P. thank the U.S. Department of Energy for its support under Contract No. DE-SC0012704. L. L. is partially supported by the U.S. Department of Energy, Office of Science, Office of Workforce Development for Teachers and Scientists, Office of Science Graduate Student Research (SCGSR) program. The SCGSR program is administered by the Oak Ridge Institute for Science and Education for the DOE under Contract No. DE-AC05-06OR23100. L. L. thanks the theory group of Brookhaven National Laboratory for their hospitality under this program. U.S. Department of Energy Office of Nuclear Physics or High Energy Physics.

APPENDIX: SPECTRAL DENSITY

The spectral densities are obtained for a generic vector boson mass M, with a straightforward application for either charged or neutral current cases.

We need to identify the regions in which the product of delta functions in (4.22) with (4.23) have support in the interval $W^- \leq W \leq W^+$.

Using the identities

$$n_f(-k) = 1 - n_f(k); \qquad N_b(-p^0) = -(1 + N_b(p^0)), \tag{A1}$$

the product

$$[\delta(k_0 - k) - \delta(k_0 + k)][\delta(q_0 - k^0 - W_p) - \delta(q_0 - k^0 + W_p)][1 - n_f(k_0) + N_b(p_0)]; \quad p^0 = q^0 - k^0 \tag{A2}$$

is gathered into four different terms; keeping the finite temperature contributions only, these are

$$\mathbf{1}):\ \delta(k^0 - k)\delta(q^0 - k - W)[-n_f(k) + N_b(q^0 - k)]. \tag{A3}$$

This contribution describes the *decay* of the sterile neutrino and its inverse process $\nu_s \leftrightarrow lW$. The delta function $\delta(q^0 - k - W)$ has support for $W^- \leq q^0 - k \leq W^+$ as a function of k, and this constraint implies

$$k^- \leq k \leq k^+; \qquad k^\pm = \frac{(q^0)^2 - q^2 - M^2}{2(q^0 \mp q)} \quad \text{for } q^0 \geq \sqrt{q^2 + M^2} \tag{A4}$$

$$\mathbf{2}):\ \delta(k^0 + k)\delta(q^0 + k + W)[1 - n_f(-k) + N_b(q^0 + k)]. \tag{A5}$$

For this term, it must be that $q^0 + k < 0$ since $W^- \leq W \leq W^+$, and because $k > 0$, it follows that $q^0 < 0$. Therefore, using the identity (A1) and keeping solely the finite temperature contributions, this term yields

$$\mathbf{2}):\ -\delta(k^0 + k)\delta(|q^0| - k - W)[-n_f(k) + N_b(|q^0| - k)]; \qquad |q^0| - k > 0, \tag{A6}$$

which is similar to the previous case. The region of support is $q^0 < 0$ and for k is

$$k^- \leq k \leq k^+; \qquad k^\pm = \frac{(q^0)^2 - q^2 - M^2}{2(|q^0| \mp q)} \quad \text{for } |q^0| \geq \sqrt{q^2 + M^2} \tag{A7}$$

$$\mathbf{3}):\ -\delta(k^0 - k)\delta(q^0 - k + W)[1 - n_f(k) + N_b(q^0 - k)]; \tag{A8}$$

this term has support for $k - q^0 > 0$, using (A1),

$$\mathbf{3}):\ \delta(k^0 - k)\delta(k - q^0 - W)[n_f(k) + N_b(k - q^0)]. \tag{A9}$$

For $q_0 > 0$, this contribution describes the decay of the charged lepton and its inverse $l \leftrightarrow \nu_s W$, whereas for $q_0 < 0$, it describes the decay of the W into a charged lepton and a sterile *antineutrino* and its inverse, namely, $W \leftrightarrow \bar{\nu}_s l$. The regions of support are

$$i):\quad 0 \leq q^0 \leq q; \qquad k^- \leq k < \infty; \qquad k^- = \frac{q^2 + M^2 - (q^0)^2}{2(q - q^0)} \tag{A10}$$

$$ii):\quad 0 > q^0 > -q; \qquad k^+ = \infty; \qquad k^- = \frac{q^2 + M^2 - (q^0)^2}{2(q - q^0)} \tag{A11}$$

$$iii):\quad q^0 < 0; \qquad q \leq |q^0| \leq \sqrt{q^2 + M^2}; \qquad k^- \leq k \leq k^+; \qquad k^\pm = \frac{q^2 + M^2 - (q^0)^2}{2(|q^0| \mp q)} \tag{A12}$$

$$\mathbf{4}):\ -\delta(k^0+k)\delta(q^0+k-W)[n_f(k)+N_b(q^0+k)]. \tag{A13}$$

For $q_0>0$, the delta function $\delta(q^0+k-W)$ describes the decay of the W into a sterile neutrino and a charged lepton. The regions of support are

$$i:\ 0\le q^0\le q:;\qquad k^-\le k<\infty;\qquad k^-=\frac{q^2+M^2-(q^0)^2}{2(q+q^0)} \tag{A14}$$

$$ii:\ q\le q^0\le\sqrt{q^2+M^2}:;\qquad k^-\le k\le k^+;\qquad k^\pm=\frac{q^2+M^2-(q^0)^2}{2(q\mp q^0)} \tag{A15}$$

$$iii:\ -q\le q^0\le 0:;\qquad k^-\le k<\infty;\qquad k^-=\frac{q^2+M^2-(q^0)^2}{2(q+q^0)} \tag{A16}$$

The regions i and iii describe the process of Landau damping [104], with support below the light cone, corresponding to emission and reabsorption of thermal excitations similarly to the case of the self-energy of quarks interacting with gluons or electrons with photons. For the case of the massive vector boson, the Landau damping cut is continued above the light cone, corresponding to the region ii. This term is the only one that contributes to the imaginary part on the mass shell of the sterilelike neutrino.

The integrals over k^0 can be done straightforwardly; the contributions from $L[Q,k]\cdot P[p]$ [see Eqs. (4.12) and (4.15)] yield the following terms for negative and positive helicity respectively:

k^0 integrals, negative helicity:
(i) for **1**: $-\frac{M^2}{q^2}[F_1(q_0,q)+kF_2(q_0,q)]$
(ii) for **2**: $-\frac{M^2}{q^2}[F_1(q_0,q)-kF_2(q_0,q)]$
(iii) for **3**: $-\frac{M^2}{q^2}[F_1(q_0,q)+kF_2(q_0,q)]$
(iv) for **4**: $-\frac{M^2}{q}[F_1(q_0,q)-kF_2(q_0,q)]$

k^0 integrals, positive helicity:
(i) for **1**: $\frac{M^2}{q^2}[G_1(q_0,q)+kG_2(q_0,q)]$
(ii) for **2**: $\frac{M^2}{q^2}[G_1(q_0,q)-kG_2(q_0,q)]$
(iii) for **3**: $\frac{M^2}{q^2}[G_1(q_0,q)+kG_2(q_0,q)]$
(iv) for **4**: $\frac{M^2}{q}[G_1(q_0,q)-kG_2(q_0,q)]$

1. k integrals

The next step is to calculate the k integrals. This is facilitated by the following identities,

$$n_f(k)=-T\frac{d}{dk}\ln[1+e^{-k/T}] \tag{A17}$$

$$N_b(q^0-k)=-T\frac{d}{dk}\ln[1-e^{k/T}e^{-q^0/T}], \tag{A18}$$

and a similar identity for $N_b(k-q^0);N_b(q^0+k)$. With these identities, we find

$$\int_{k^-}^{k^+}n_f(k)dk=-T\ln\left[\frac{1+e^{-k^+/T}}{1+e^{-k^-/T}}\right] \tag{A19}$$

$$\int_{k^-}^{k^+}N_b(q^0-k)dk=-T\ln\left[\frac{1-e^{k^+/T}e^{-q^0/T}}{1-e^{k^-/T}e^{-q^0/T}}\right] \tag{A20}$$

$$\int_{k^-}^{k^+}N_b(k-q^0)dk=T\ln\left[\frac{1-e^{-k^+/T}e^{q^0/T}}{1-e^{-k^-/T}e^{q^0/T}}\right] \tag{A21}$$

$$\int_{k^-}^{k^+}kn_f(k)dk=-T^2\Big\{k^+\ln[1+e^{-k^+/T}]-k^-\ln[1+e^{-k^-/T}]-\sum_{n=1}^{\infty}\frac{(-1)^n}{n^2}[e^{-nk^+/T}-e^{-nk^-/T}]\Big\} \tag{A22}$$

$$\int_{k^-}^{k^+}kN_b(q^0-k)dk=-T^2\Big\{k^+\ln[1-e^{k^+/T}e^{-q^0/T}]-k^-\ln[1-e^{k^-/T}e^{-q^0/T}]+\sum_{n=1}^{\infty}\frac{e^{-nq^0/T}}{n^2}[e^{nk^+/T}-e^{nk^-/T}]\Big\} \tag{A23}$$

$$\int_{k^-}^{k^+}kN_b(k-q^0)dk=-T^2\{-k^+\ln[1-e^{-k^+/T}e^{q^0/T}]+k^-\ln[1-e^{-k^-/T}e^{q^0/T}]+\sum_{n=1}^{\infty}\frac{e^{nq^0/T}}{n^2}[e^{-nk^+/T}-e^{-nk^-/T}]\}. \tag{A24}$$

In the integrals (A22)–(A24), we have used the identities (A17), (A18), integrated by parts, expanded the logarithms in power series and integrated term by term. The infinite sums can be expressed in terms of dilogarithmic (Spence's) functions, but such form is not particularly useful.

2. Numerical implementation for the real part

The numerical implementation for the real parts from the dispersive form (2.14) is best achieved in a "modular form," which is facilitated by introducing

$$\int_{k^-}^{k^+}[N_b(q^0-k)-n_f(k)]dk\equiv -TD1(q^0,q) \tag{A25}$$

$$\int_{k^-}^{k^+}[N_b(q^0-k)-n_f(k)]kdk \equiv -T^2 Dk1(q^0,q) \tag{A26}$$

$$\int_{k^-}^{k^+}[N_b(k-q^0)+n_f(k)]dk \equiv -TD2(q^0,q) \tag{A27}$$

$$\int_{k^-}^{k^+}[N_b(k-q^0)+n_f(k)]kdk \equiv -T^2 Dk2(q^0,q), \tag{A28}$$

where the respective integrals are given above. In terms of these quantities and $F_{1,2}(q^0,q)$ defined by Eqs. (4.13) and (4.14) [and $G_{1,2}$ defined by Eqs. (4.16) and (4.17) for positive helicity], we find for negative helicity the following contributions to the imaginary parts in the different regions 1–4 of q^0 defined by the support of the corresponding delta functions described above,

$$\mathrm{Im}\Sigma^{(1)} = \frac{g^2M^2T}{16\pi q^2}[F_1(q^0,q)D1(q^0,q)+TF_2(q^0,q)Dk1(q^0,q)]; \qquad q^0 \geq \sqrt{q^2+M^2} \tag{A29}$$

$$\mathrm{Im}\Sigma^{(2)} = -\frac{g^2M^2T}{16\pi q^2}[F_1(q^0,q)D1(|q^0|,q)-TF_2(q^0,q)Dk1(|q^0|,q)]; \qquad q^0<0, \qquad |q^0| \geq \sqrt{q^2+M^2} \tag{A30}$$

$$\begin{aligned}\mathrm{Im}\Sigma^{(3)} = \frac{g^2M^2T}{16\pi q^2}\{&[F_1(q^0,q)D2(q^0,q)+TF_2(q^0,q)Dk2(q^0,q)](0<q^0<q)\\ &+[F_1(q^0,q)D2(q^0,q)+TF_2(q^0,q)Dk2(q^0,q)](0>q^0>-q)\\ &+[F_1(q^0,q)D2(q^0,q)+TF_2(q^0,q)Dk2(q^0,q)](-q>q^0>-\sqrt{k^2+M^2})\}\end{aligned} \tag{A31}$$

in the first two terms $k^+=\infty \to D2(k^+=\infty)=Dk2(k^+=\infty)=0$ and only the lower limit with k^- corresponding to the case 3 above contributes, the two limits $k^\pm$ contribute to the last term,

$$\begin{aligned}\mathrm{Im}\Sigma^{(4)} = -\frac{g^2M^2T}{16\pi q^2}\{&[F_1(q^0,q)D2(-q^0,q)-TF_2(q^0,q)Dk2(-q^0,q)](0<q^0<q)\\ &+[F_1(q^0,q)D2(-q^0,q)-TF_2(q^0,q)Dk2(-q^0,q)](q<q^0<\sqrt{k^2+M^2})\\ &+[F_1(q^0,q)D2(-q^0,q)-TF_2(q^0,q)Dk2(-q^0,q)](0>q^0>-q)\}.\end{aligned} \tag{A32}$$

Now, the real part of the self-energy is calculated with the dispersive form (2.14) with

$$\mathrm{Im}\Sigma(q^0,q) = \mathrm{Im}\Sigma^{(1)}(q^0,q)+\mathrm{Im}\Sigma^{(2)}(q^0,q)+\mathrm{Im}\Sigma^{(3)}(q^0,q)+\mathrm{Im}\Sigma^{(4)}(q^0,q). \tag{A33}$$

In each region in q^0, the values of $k^\pm$ are given by the different cases analyzed above. The principal part is obtained by excising an interval of width 2ϵ around $q^0=q$ with $\epsilon \ll 1$.

For positive helicity, the same analysis above holds with the following modifications:

(i) $M^2 \to -M^2$ *only in the prefactor*

(ii) $F_{1,2}(q^0,q) \to G_{1,2}(q^0,q)$ where $F_{1,2}$ and $G_{1,2}$ are given by Eqs. (4.13) and (4.14) and (4.16) and (4.17), respectively. Note that $F_{1,2}$ and $G_{1,2}$ obey the relation (4.18).

Finally, we introduce the dimensionless variables,

$$z = q^0/T; \qquad y = q/T; \qquad \tau = M_W/T, \tag{A34}$$

where, as discussed in the text, we use M_W as the baseline scale. The integrals over q^0 are then rendered dimensionless in terms of these variables. The dispersive integrals over the dimensionless variable z are carried out numerically, and the final results for the real part of the self-energy are generically of the form

$$\mathrm{Re}\Sigma^{\pm}(q) = \frac{g^2M^2T}{16\pi^2q^2}\mathcal{K}^{\pm}[\tau,y], \tag{A35}$$

where $\mathcal{K}^{\pm}[\tau,y]$ are dimensionless functions of τ, y that are obtained numerically with the procedure detailed above. For charged currents, $g^2=g_w^2/2$, $M=M_W$; for neutral currents, $g^2=g_w^2/(2c)^2, M=M_W/c, c=\cos(\theta_w)\simeq 0.88$; and for neutral currents, $\tau \to \tau/c$ in the argument of $\mathcal{K}[\tau,y]$.

3. Low temperature limit

In the low temperature limit, $M_W \gg T$, and keeping only the finite temperature contributions and using the identities (A1), we can neglect N_b. In (4.8), the product of delta functions and distribution functions becomes

$$n_f(k)\{\delta(k^0-k)[\delta(q^0-k+W_p)-\delta(q^0-k-W_p)]+\delta(k^0+k)[\delta(q^0+k+W_p)-\delta(q^0+k-W_p)]\}. \tag{A36}$$

Now, it is more convenient to integrate over q^0 and k^0 in the dispersive integral (2.14), leaving only the integrals in k, with

$$d^3k=(2\pi)k^2dkd(\cos(\varphi)) \tag{A37}$$

with φ the angle between $\vec{q}$ and $\vec{k}$.

For negative helicity, we find

$$L_{\mu\nu}[Q^+,k]P^{\mu\nu}[p]=k(1-\cos(\varphi))+\frac{2k}{M^2}(q^0-q\cos(\varphi))(q^0-k-q+k\cos(\varphi)); \quad \text{for } k^0=k \tag{A38}$$

$$L_{\mu\nu}[Q^+,k]P^{\mu\nu}[p]=-k(1+\cos(\varphi))-\frac{2k}{M^2}(q^0+q\cos(\varphi))(q^0+k-q+k\cos(\varphi)); \quad \text{for } k^0=-k. \tag{A39}$$

Integrating over q^0, and implementing the delta functions and expanding the numerator and denominator in powers of k/M, q/M, integrating over $\cos(\varphi)$, keeping only the leading order terms (proportional to $1/M^4$) and using

$$\int_0^\infty k^3 n_f(k)dk=\frac{7\pi^4T^4}{120}, \tag{A40}$$

we find for negative helicity

$$\mathrm{Re}\Sigma^-(q)=\frac{14\pi^2}{90}g^2\left(\frac{T}{M}\right)^4 q. \tag{A41}$$

For positive helicity, we follow the same steps, with

$$L_{\mu\nu}[Q^-,k]P^{\mu\nu}[p]=k(1+\cos(\varphi))+\frac{2k}{M^2}(q^0-q\cos(\varphi))(q^0-k+q-k\cos(\varphi)); \quad \text{for } k^0=k \tag{A42}$$

$$L_{\mu\nu}[Q^-,k]P^{\mu\nu}[p]=-k(1-\cos(\varphi))-\frac{2k}{M^2}(q^0+q\cos(\varphi))(q^0+k+q-k\cos(\varphi)); \quad \text{for } k^0=-k. \tag{A43}$$

Following the same steps as for negative helicity, we find

$$\mathrm{Re}\Sigma^+(q)=\frac{14\pi^2}{180}g^2\left(\frac{T}{M}\right)^4 q. \tag{A44}$$

[1] W. J. G. de Blok, Adv. Astron. **2010**, 789293 (2010).
[2] J. Dalcanton and C. Hogan, Astrophys. J. **561**, 35 (2001); C. Hogan and J. Dalcanton, Phys. Rev. D **62**, 063511 (2000).
[3] M. Boylan-Kolchin, J. Bullock, and M. Kaplinghat, Mon. Not. R. Astron. Soc. **415**, L40 (2011); S. Garrison-Kimmel, M. Boylan-Kolchin, J. Bullock, and E. Kirby, Mon. Not. R. Astron. Soc. **444**, 222 (2014); E. Papastergis, R. Giovanelli, M. Haynes, and F. Shankar, Astron. Astrophys. **574**, A113 (2015).
[4] M. G. Walker and J. Penarrubia, Astrophys. J. **742**, 20 (2011).
[5] A. V. Tikhonov and A. Klypin, Mon. Not. R. Astron. Soc. **395**, 1915 (2009).
[6] A. V. Tikhonov, S. Gottlober, G. Yepes, and Y. Hoffman, Mon. Not. R. Astron. Soc. **399**, 1611 (2009).
[7] B. Moore, T. Quinn, R. Governato, J. Stadel, and G. Lake, Mon. Not. R. Astron. Soc. **310**, 1147 (1999).
[8] P. Bode, J. P. Ostriker, and N. Turok, Astrophys. J. **556**, 93 (2001).

[9] V. Avila-Reese, P. Colin, O. Valenzuela, E. D'Onghia, and C. Firmani, Astrophys. J. **559**, 516 (2001).
[10] M. Lovell, C. Frenk, V. Eke, A. Jenkins, L. Gao, and T. Theuns, Mon. Not. R. Astron. Soc. **439**, 300 (2014).
[11] S. Dodelson and L. M. Widrow, Phys. Rev. Lett. **72**, 17 (1994).
[12] S. Colombi, S. Dodelson, and L. M. Widrow, Astrophys. J. **458**, 1 (1996).
[13] A. D. Dolgov and S. H. Hansen, Astropart. Phys. **16**, 339 (2002).
[14] K. Abazajian, G. Fuller, and M. Patel, Phys. Rev. D **64**, 023501 (2001).
[15] K. Abazajian *et al.*, arXiv:1204.5379.
[16] A. Kusenko, Phys. Rep. **481**, 1 (2009).
[17] A. Boyarsky, D. Iakubovskyi, and O. Ruchayskiy, Phys. Dark Univ. **1**, 136 (2012); A. Boyarsky, O. Ruchayskiy, and M. Shaposhnikov, Annu. Rev. Nucl. Part. Sci. **59**, 191 (2009).
[18] S. Paduroiu, Y. Revaz, and D. Pfenniger, arXiv: 1506.03789; A. V. Maccio, S. Paduroiu, D. Anderhalden, A. Schneider, and B. Moore, Mon. Not. R. Astron. Soc. **424**, 1105 (2012); S. Shao, L. Gao, T. Theuns, and C. Frenk, Mon. Not. R. Astron. Soc. **430**, 2346 (2013).
[19] P. Ade *et al.* (Planck Collaboration), Astron. Astrophys. **571**, A16 (2014).
[20] R. Barbieri and A. D. Dolgov, Nucl. Phys. **B349**, 743 (1991); Phys. Lett. B **237**, 440 (1990); K. Kainulainen, Phys. Lett. B **244**, 191 (1990); K. Enqvist, K. Kainulainen, and J. Maalampi, Phys. Lett. B **249**, 531 (1990); Nucl. Phys. **B349**, 754 (1991); K. Enqvist, K. Kainulainen, and M. Thomson, Nucl. Phys. **B373**, 498 (1992).
[21] A. D. Dolgov, Phys. Rep. **370**, 333 (2002); Phys. At. Nucl. **71**, 2152 (2008); Surv. High Energy Phys. **17**, 91 (2002).
[22] X. Shi and G. Fuller, Phys. Rev. Lett. **82**, 2832 (1999).
[23] T. Asaka, M. Laine, and M. Shaposhnikov, J. High Energy Phys. 01 (2007) 091; 06 (2006) 053.
[24] J. Ghiglieri and M. Laine, J. High Energy Phys. 11 (2015) 171; I. Ghisoiu and M. Laine, J. Cosmol. Astropart. Phys. 12 (2014) 032; M. Laine and M. Shaposhnikov, J. Cosmol. Astropart. Phys. 06 (2008) 031.
[25] M. Laine and M. Meyer, J. Cosmol. Astropart. Phys. 07 (2015) 035.
[26] J. Ghiglieri and M. Laine, J. Cosmol. Astropart. Phys. 07 (2016) 015.
[27] T. Venumadhav, F.-Y. Cyr-Racine, K. N. Abazajian, and C. M. Hirata, Phys. Rev. D **94**, 043515 (2016).
[28] D. Boyanovsky, Phys. Rev. D **78**, 103505 (2008).
[29] K. Petraki and A. Kusenko, Phys. Rev. D **77**, 065014 (2008).
[30] K. Petraki, Phys. Rev. D **77**, 105004 (2008).
[31] A. Merle, Int. J. Mod. Phys. D **22**, 1330020 (2013); A. Merle and A. Schneider, Phys. Lett. B **749**, 283 (2015); A. Merle and M. Totzauer, J. Cosmol. Astropart. Phys. 06 (2015) 011; A. Merle, V. Niro, and D. Schmidt, J. Cosmol. Astropart. Phys. 03 (2014) 028.
[32] M. Drewes and J. U. Kang, J. High Energy Phys. 05 (2016) 051.
[33] C. R. Watson, Z. Li, and N. K. Polley, J. Cosmol. Astropart. Phys. 03 (2012) 018; H. Yuksel, J. F. Beacom, and C. R. Watson, Phys. Rev. Lett. **101**, 121301 (2008).
[34] E. Bulbul, M, Markevitch, A. Foster, R. Smith, M. Loewenstein, and S. Randall, Astrophys. J. **789**, 13 (2014).
[35] A. Boyarsky, O. Ruchayskiy, D. Iakubovskyi, and J. Franse, Phys. Rev. Lett. **113**, 251301 (2014); A. Boyarsky, J. Franse, D. Iakubovskyi, and O. Ruchayskiy, Phys. Rev. Lett. **115**, 161301 (2015).
[36] T. Jeltema and S. Profumo, Mon. Not. R. Astron. Soc. **450**, 2143 (2015); T. Jeltema and S. Profumo, arXiv:1411.1759.
[37] D. Malyshev, A. Neronov, and D. Eckert, Phys. Rev. D **90**, 103506 (2014).
[38] M. E. Anderson, E. Churazov, and J. N. Bregman, Mon. Not. R. Astron. Soc. **452**, 3905 (2015).
[39] N. Sekiya, N. Y. Yamasaki, and K. Mitsuda, arXiv: 1504.02826.
[40] K. Abazajian, Phys. Rev. Lett. **112**, 161303 (2014).
[41] K. Abazajian and G. Fuller, Phys. Rev. D **66**, 023526 (2002).
[42] K. Abazajian, Phys. Rev. Lett. **112**, 161303 (2014).
[43] S. Horiuchi, P. Humphrey, J. Onorbe, K. Abazajian, M. Kaplinghat, and S. Garrison-Kimmel, Phys. Rev. D **89**, 025017 (2014).
[44] M. Kaplinghat, R. Lopez, S. Dodelson, and R. Scherrer, Phys. Rev. D **60**, 123508 (1999).
[45] L. Lello and D. Boyanovsky, Phys. Rev. D **91**, 063502 (2015).
[46] K. C. Y. Ng, S. Horiuchi, J. M. Gaskins, M. Smith, and R. Preece, Phys. Rev. D **92**, 043503 (2015).
[47] A. Merle, A. Schneider, and M. Totzauer, J. Cosmol. Astropart. Phys. 04 (2016) 003.
[48] K. A. Olive *et al.* (Particle Data Group Collaboration), Chin. Phys. C **38**, 090001 (2014).
[49] A. Balantekin and W. Haxton, Prog. Part. Nucl. Phys. **71**, 150 (2013).
[50] H. Minakata, arXiv:1403.3276.
[51] A. Aguilar-Arevalo *et al.* (LSND Collaboration), Phys. Rev. D **64**, 112007 (2001).
[52] A. A. Aguilar-Arevalo *et al.* (MiniBooNE Collaboration), Phys. Rev. Lett. **110**, 161801 (2013); arXiv:1303.2588.
[53] A. Mirizzi, N. Saviano, G. Miele, and P. D. Serpico, Phys. Rev. D **86**, 053009 (2012).
[54] C. Giunti, arXiv:1311.1335.
[55] F. P. An *et al.* (Daya Bay Collaboration) Phys. Rev. Lett. **113**, 141802 (2014); I. Girardi, D. Meloni, T. Ohlsson, H. Zhang, and S. Zhou, J. High Energy Phys. 08 (2014) 057.
[56] D. Boyanovsky and L. Lello, New J. Phys. **16**, 063050 (2014); D. Boyanovsky, Nucl. Phys. **B888**, 248 (2014); arXiv:1409.4265.
[57] L. Lello and D. Boyanovsky, Phys. Rev. D **87**, 073017 (2013).
[58] R. E. Shrock, Phys. Rev. D **24**, 1232 (1981); **24**, 1275 (1981); Phys. Lett. **96B**, 159 (1980).
[59] V. Barger, R. J. N. Phillips, and S. Sarkar, Phys. Lett. B **352**, 365 (1995).
[60] T. Lasserre, Phys. Dark Univ. **4**, 81 (2014).
[61] S. Gariazzo, C. Giunti, and M. Laveder, arXiv:1404.6160.
[62] S. N. Gninenko, Phys. Rev. D **83**, 093010 (2011); **85**, 051702 (2012); Phys. Lett. B **710**, 86 (2012); S. N. Gninenko, D. S. Gorbunov, and M. E. Shaposhnikov, Adv. High Energy Phys. **2012**, 718259 (2012).

[63] C. Dib, J. Helo, M. Hirsch, S. Kovalenko, and I. Schmidt, Phys. Rev. D **85**, 011301 (2012).
[64] G. Cvetic, C. S. Kim, R. Kogerler, and J. Zamora-Saa, Phys. Rev. D **92**, 013015 (2015).
[65] D. Boyanovsky, Phys. Rev. D **90**, 105024 (2014).
[66] W.-Y. Keung and G. Senjanovic, Phys. Rev. Lett. **50**, 1427 (1983); V. Tello, M. Nemevsek, F. Nesti, G. Senjanovic, and F. Vissani, Phys. Rev. Lett. **106**, 151801 (2011); G. Senjanovic and V. Tello, *Proc. Sci.*, PLANCK2015 (2016) 141.
[67] S. Banerjee, P. S. Bhupal Dev, A. Ibarra, T. Mandal, and M. Mitra, Phys. Rev. D **92**, 075002 (2015).
[68] J. N. Ng, A. de la Puente, and B. W.-P. Pan, J. High Energy Phys. 12 (2015) 172.
[69] A. Atre, T. Han, S. Pascoli, and B. Zhang, J. High Energy Phys. 05 (2009) 030; T. Han and B. Zhang, Phys. Lett. **97B**, 171804 (2006); J. Gluza and T. Jelinski, Phys. Lett. B **748**, 125 (2015); J. Gluza, T. Jelinski, and R. Szafron, Phys. Rev. D **93**, 113017 (2016); P. Coloma, B. Dobrescu, and J. Lopez-Pavon, Phys. Rev. D **92**, 115023 (2015); P. S. Bhupal Dev and R. N. Mohapatra, Phys. Rev. Lett. **115**, 181803 (2015).
[70] P. S. Bhupal Dev, A. Pilaftsis, and U. Yang, Phys. Rev. Lett. **112**, 081801 (2014); F. F. Deppisch, P. S. Bhupal Dev, and A. Pilaftsis, New J. Phys. **17**, 075019 (2015); A. Das, P. S. Bhupal Dev, and N. Okada, Phys. Lett. B **735**, 364 (2014); A. Das and N. Okada, Phys. Rev. D **88**, 113001 (2013).
[71] W. Bonivento *et al.*, arXiv:1310.1762.
[72] G. M. Fuller, C. T. Kishimoto, and A. Kusenko, arXiv: 1110.6479; A. V. Patwardhan, G. M. Fuller, C. T. Kishimoto, and A. Kusenko, Phys. Rev. D **92**, 103509 (2015).
[73] G. Gelmini, E. Osoba, S. Palomares-Ruiz, and S. Pascoli, J. Cosmol. Astropart. Phys. 10 (2008) 029.
[74] H. Ishida, M. Kusakabe, and H. Okada, Phys. Rev. D **90**, 083519 (2014).
[75] For a review, see B. D. Fields, Ann. Rev. Nucl. Part. Sci. **61**, 47 (2011); arXiv:1203.3551.
[76] F. Iocco, G. Mangano, G. Miele, O. Pisanti, and P. D. Serpico, Phys. Rep. **472**, 1 (2009).
[77] M. Pospelov and J. Pradler, Annu. Rev. Nucl. Part. Sci. **60**, 539 (2010).
[78] V. Poulin and P. D. Serpico, Phys. Rev. Lett. **114**, 091101 (2015); Phys. Rev. D **91**, 103007 (2015).
[79] L. Salvati, L. Pagano, M. Lattanzi, M.Gerbino, and A. Melchiorri, J. Cosmol. Astropart. Phys. 08 (2016) 022.
[80] S. H. Hansen and Z. Haiman, Astrophys. J. **600**, 26 (2004).
[81] A. Kusenko, S. Pascoli, and D. Semikoz, J. High Energy Phys. 11 (2005) 028.
[82] O. Ruchayskiy and A. Ivashko, J. High Energy Phys. 06 (2012) 100.
[83] A. C. Vincent, E. Fernandez- Martinez, P. Hernandez, M. Lattanzi, and O. Mena, J. Cosmol. Astropart. Phys. 04 (2015) 006.
[84] T. Asaka, M. Shaposhnikov, and A. Kusenko, Phys. Lett. B **638**, 401 (2006); T. Asaka and M. Shaposhnikov, Phys. Lett. B **620**, 17 (2005).
[85] M. Drewes, *Proc. Sci.*, EPS-HEP2015 (2015) 075; M. Drewes and B. Garbrecht, arXiv:1502.00477.
[86] E. Izaguirre, G. Krnjaic, and M. Pospelov, Phys. Rev. D **92**, 095014 (2015).
[87] K. R. Dienes and B. Thomas, Phys. Rev. D **85**, 083523 (2012); **85**, 083524 (2012); K. R. Dienes, J. Kumar, B. Thomas, and D. Yaylali, Phys. Rev. Lett. **114**, 051301 (2015).
[88] A. Boyarsky, J. Lesgourgues, O. Ruchayskiy, and M. Viel, J. Cosmol. Astropart. Phys. 05 (2009) 012.
[89] L. Lello and D. Boyanovsky, J. Cosmol. Astropart. Phys. 06 (2016) 011.
[90] L. Wolfenstein, Phys. Rev. D **17**, 2369 (1978); S. P. Mikheev and A. Y. Smirnov, Yad. Fiz. **42**, 1441 (1985) [Sov. J. Nucl. Phys. **42**, 913 (1985)].
[91] P. Minkowski, Phys. Lett. **67B**, 421 (1977); M. Gell-Mann, P. Ramond, and R. Slansky, *Supergravity*, edited by P. van Nieuwenhuizen and D. Freedman (North-Holland, Amsterdam, 1979), p. 315; R. N. Mohapatra and G. Senjanovic, Phys. Rev. Lett. **44**, 912 (1980); M. Fukugita and T. Yanagida, *Physics of Neutrinos* (Springer, Berlin, 2003).
[92] J. Wu, C.-M. Ho, and D. Boyanovsky, Phys. Rev. D **80**, 103511 (2009).
[93] C. M. Ho, D. Boyanovsky, and H. J. de Vega, Phys. Rev. D **72**, 085016 (2005).
[94] C. M. Ho and D. Boyanovsky, Phys. Rev. D **73**, 125014 (2006).
[95] D. Boyanovsky, K. Davey, and C. M. Ho, Phys. Rev. D **71**, 023523 (2005).
[96] D. Boyanovsky, New J. Phys. **17**, 063017 (2015).
[97] H. A. Weldon, Phys. Rev. D **28**, 2007 (1983).
[98] M. Le Bellac, *Thermal Field Theory*, Cambridge Monographs on Mathematical Physics (Cambridge University Press, Cambridge, England, 1996).
[99] E. Braaten and R. Pisarski, Nucl. Phys. **B337**, 569 (1990); Nucl. Phys. **B339**, 310 (1990); Phys. Rev. Lett. **64**, 1338 (1990); Phys. Rev. D **42**, 2156 (1990); **45**, R1827 (1992); **46**, 1829 (1992).
[100] R. Pisarski, Nucl. Phys. **A544**, 527C (1992); Can. J. Phys. **71**, 280 (1993); Phys. Rev. Lett. **63**, 1129 (1989); R. Pisarski, Physica (Amsterdam) **158A**, 246 (1989).
[101] J. Frenkel and J. C. Taylor, Nucl. Phys. **B334**, 199 (1990).
[102] H. A. Weldon, Phys. Rev. D **26**, 1394 (1982); **26**, 2789 (1982).
[103] D. Notzold and G. Raffelt, Nucl. Phys. **B307**, 924 (1988); P. B. Pal and T. N. Pham, Phys. Rev. D **40**, 259 (1989).
[104] R. D. Pisarski, Nucl. Phys. **A498**, 423 (1989).
[105] D. Gorbunov and M. Shaposhnikov, J. High Energy Phys. 10 (2007) 015.
[106] P. B. Pal and L. Wolfenstein, Phys. Rev. **25**, 766 (1982).
[107] B. Audren, J. Lesgourgues, G. Mangano, P. D. Serpico, and T. Tram, J. Cosmol. Astropart. Phys. 12 (2014) 028.
[108] V. Poulin, P. D. Serpico, and J. Lesgourgues, J. Cosmol. Astropart. Phys. 08 (2016) 036.
[109] R. R. Volkas and Y. Y. Y. Wong, Phys. Rev. D **62**, 093024 (2000); K. S. M. Lee, R. R. Volkas, and Y. Y. Y. Wong, Phys. Rev. D **62**, 093025 (2000).
[110] P. Hernandez, M. Kekic, and J. Lopez-Pavon, Phys. Rev. D **90**, 065033 (2014).
[111] R. Adhikari *et al.* J. Cosmol. Astropart. Phys. 01 (2017) 025.